QA

OCRWM	SCIENTIFIC ANALYSIS COVER SHEET	1. QA: QA Page 1 of 82

DOC.20030916.0008

2. Scientific Analyses Title Saturated Zone Colloid Transport	DOC.20030916.0008
3. DI (including Revision Number) ANL-NBS-HS-000031 REV01	
4. Total Attachments N/A	5. Attachment Numbers - Number of pages in each N/A

	Printed Name	Signature	Date
6. Originator	H.S. Viswanathan, P. W. Reimus	SIGNATURE ON FILE	9-04-03
7. Checker	A. Abdel-Fattah	SIGNATURE ON FILE	9-04-03
8. QER	J. Heaney	SIGNATURE ON FILE	9-05-03
9. Responsible Manager/Lead	S. P. Kuzio	SIGNATURE ON FILE	9-05-03
10. Responsible Manager	P. R Dixon	SIGNATURE ON FILE	9-05-03

11. Remarks

TER-02-0061, although originally designated as being resolved by this AMR, is addressed in MDL-NBS-HS-000010 REV 01.

Revision History

12. Revision/ICN No.	13. Description of Revision/Change
REV 00	Initial Issue
REV 00 ICN 01	REV 00 ICN 01 of this AMR incorporated the updating of technical information and editorial changes.
REV 01	REV 01 includes additional field and laboratory analysis. Change bars were not used because the changes were extensive.

CONTENTS

Page

CONTENTS (Continued)

Page

INTENTIONALLY LEFT BLANK

FIGURES

Page

FIGURES (Continued)

Page

TABLES

Page

TABLES (Continued)

Page

ACRONYMS AND ABBREVIATIONS

ATC	Alluvial Testing Complex
BSC	Bechtel/SAIC Company
CDF	cumulative distribution function
CML	carboxylate-modified latex
CRWMS M&O	Civilian Radioactive Waste Management System Management and Operating Contractor
DIRS	Document Input Reference System
DOE	U.S. Department of Energy
DTN	data tracking number
FEPs	features, events, and processes
NTS	Nevada Test Site
NRC	U.S. Nuclear Regulatory Commission
OCRWM	Office of Civilian Radioactive Waste Management
PA	Performance Assessment
QA	quality assurance
SCM	Software Configuration Management
STN	software tracking number
SZ	saturated zone
TBD	to be determined
TBV	to be verified
TSPA	Total Systems Performance Assessment
TSPA-LA	Total Systems Performance Assessment for the License Application
TSPA-SR	Total Systems Performance Assessment for the Site Recommendation
UZ	unsaturated zone
V	version
YMP	Yucca Mountain Project
YMRP	Yucca Mountain Review Plan

INTENTIONALLY LEFT BLANK

1. PURPOSE

The purpose of this scientific analysis is to provide retardation factors for colloids transporting in the saturated zone (SZ). Because radionuclides such as Pu and Am sorb mostly irreversibly to colloids, the colloid retardation factors developed in this analysis are needed to simulate the irreversibly sorbed colloids that exist in the colloid-facilitated transport model (will be discussed in the upcoming model report *Site-Scale Saturated Zone Transport* (BSC 2003 [162419])). Although it is not exclusive to any particular radionuclide release scenario, this scientific analysis especially addresses those scenarios pertaining to evidence from waste-degradation experiments, which indicate that Pu and Am may be irreversibly attached to colloids for the time scales of interest. A section of this report will also discuss the validity of using microspheres as analogs to colloids in some of the lab and field experiments used to obtain the colloid retardation factors.

This report establishes the requirements and elements of the design of a methodology for calculating colloid transport in the SZ at Yucca Mountain. Field experiments in fractured tuff at Yucca Mountain and in porous media at other sites indicate that colloids experience retardation relative to the mean pore-water velocity, suggesting that contaminants associated with colloids should also experience some retardation. Therefore, this analysis incorporates experimental and field data where available for estimating plausible ranges of retardation factors in both saturated fractured tuff and saturated alluvium. The distribution of retardation factors for tuff and alluvium are developed in a form consistent with the Performance Assessment (PA) analysis framework for simulating colloid-facilitated radionuclide transport in the SZ.

To improve on the work performed so far for the saturated-zone flow and transport modeling, effort has been made to quantify physical and chemical colloid filtration in both fractured tuff and alluvium. The filtration is simulated with a retardation factor that is developed from field and laboratory results. The fractured tuff analysis uses recent experimental data and interpretation from the C-wells reactive tracer testing complex in the SZ of Yucca Mountain to develop the retardation factor distribution. For the alluvium system, recent experimental data as well as field data from the literature are used to develop the retardation-factor distribution. The parameters derived in this report are developed in a manner consistent with the PA methodology and can be readily integrated into that analysis. The parameters have been developed in accordance with the *Scientific Processes Guidelines Manual* (BSC 2002 [160313], p. A-10) and the *Total System Performance Assessment-License Application Methods and Approach* (BSC 2002 [160146], Section 3-5).

The RELAP computer code (Software Tracking Number (STN): 10551-2.0-00 [159065]) was used in this report rather than the previously developed code RTA V1.1 (Software Tracking Number (STN): 10032-1.1-00). RELAP is more appropriate for fitting the experiments described in this model report than RTA V1.1. RELAP was developed in this analysis with a specific goal of interpreting colloid transport parameters in fractured tuff at Yucca Mountain. Microsoft Excel 2000 was used to develop retardation-factor distributions for the alluvium since experimental and field data are now available. (Note: The six-digit numerical identifier in brackets next to each reference callout throughout this report is the Yucca Mountain Project's (YMP) Document Input Reference System [DIRS] number, the purpose of which is to assist the reader in locating a specific reference in the DIRS database.)

This scientific analysis is governed by the Office of Civilian Radioactive Waste Management (OCRWM) *Technical Work Plan For: Saturated Zone Flow and Transport Modeling and Testing*, TWP-NBS-MD-000001 (BSC 2003 [163965]), Work Package ASZM04. All activities listed in the technical work plan are documented in this report.

2. QUALITY ASSURANCE

Development of this scientific analysis report and the supporting analyses have been determined to be subject to the YMP quality assurance (QA) program (BSC 2003 [163965], Section 8, Work Package ASZM04). Approved QA procedures identified in the technical work plan (BSC 2003 [163965], Section 4) have been used to conduct and document the activities described in this scientific analysis report. The technical work plan also identifies the methods used to control the electronic management of data (BSC 2003 [163965], Section 8).

This analysis reports on the saturated zone natural barrier, which is important to the demonstration of compliance with the post-closure performance objectives prescribed in 10 CFR 63.113. Therefore, it is classified as a "Quality Level – 1" with regard to importance to waste isolation, as defined in AP-2.22Q, *Classification Criteria and Maintenance of the Monitored Geologic Repository Q-List*. The report contributes to the analysis and modeling data used to support performance assessment; the conclusions do not directly impact engineered features important to safety, as defined in AP-2.22Q.

INTENTIONALLY LEFT BLANK

3. USE OF SOFTWARE

3.1 SOFTWARE TRACKED BY CONFIGURATION MANAGEMENT

The computer code used directly in this scientific analysis is listed in Table 1. This software was obtained from Software Configuration Management and is appropriate for the application. This qualified code was used only within the range of validation as required by AP-SI.1Q, *Software Management*.

Table 1. Computer Software

Software Title/Version	Software Tracking Number	Code Usage	Computer, Type, Platform, and Location	Date Baselined
RELAP V 2.0	10551-2.0-00	This software models tracer transport by convoluting a Laplace-domain transfer function for transport through dual-porosity media with transfer functions that describe tracer injection, mixing in the injection and production wellbores (or flow manifolds in laboratory experiments), and recirculation of the product fluid (in field experiments only). It also performs curve fits to field or laboratory tracer test data to obtain the best-fitting transport parameter values.	PC, Windows 2000/NT Location: Los Alamos National Laboratory (LANL)	05/21/2002

NOTE: The input and output RELAP 2.0 files are documented in the Technical Data Management System (TDMS) and identified by the following data tracking numbers (DTNs): LA0303PR831231.003, LA0303PR831352.002, LA0303PR831352.003, LA0303PR831361.001.

3.2 EXEMPT SOFTWARE

Commercial, off-the-shelf software used in support of this scientific analysis report is listed in Table 2. This software is exempt from the requirements of AP-SI.1Q, *Software Management*.

Table 2. Exempt Software

Software Name and Version (V)	Description	Computer and Platform Identification
Microsoft Excel, 2000	The commercial software, Microsoft Excel, 2000, was used for statistical analysis of data and plotting graphs. Only built-in standard functions in this software were used. No software routines or macros were used with this software to prepare this report. The output was visually checked for correctness, and the results of all calculations were hand-checked.	PC, Windows 2000/NT

NOTE: The formula and calculations performed in Microsoft Excel 2000 are too detailed to be included in this report but are documented in Notebook SN-LANL-SCI-297-V1 (Viswanathan 2003[163757]). Section 6 presents the formulae used to calculate the retardation factors. Built in EXCEL functions were used in this analysis.

INTENTIONALLY LEFT BLANK

4. INPUTS

4.1 DATA AND PARAMETERS

Input information used in this analysis comes from several sources, which are summarized in Table 3, along with their data tracking numbers (DTNs). Note that all input in Table 3 is direct input. The data are fully appropriate for the discussion of colloid transport in the fractured volcanics and alluvium in this scientific analysis report. The qualification status of the input sources is provided in the TDMS. Uncertainty of the input parameters is discussed in Section 7.3.

This report may be affected by technical product input information that requires confirmation. Any changes to the document that may occur as a result of completing the confirmation activities will be reflected in subsequent revisions. The status of the input information quality may be confirmed by review of the DIRS database.

Table 3. Direct Inputs

Data Description	Data Tracking Number	Data Used
Solute and microsphere responses from the Bullfrog Tuff tracer test at the C-wells.	LA0007PR831231.001	S00349_001-004
Solute and microsphere responses from the Prow Pass Tuff tracer test at the C-wells.	LAPR831231AQ99.001	S99126_001-004
Microsphere responses in ER-20-6 #3 in the BULLION forced-gradient experiment on Pahute Mesa, Nevada Test Site (NTS).	LA0302PR831352.002	S03120_001
Microsphere responses in ER-20-6 #2 in the BULLION forced-gradient experiment on PahuteMesa, NTS	LA0302PR831352.001	S03119_001
Solute responses in ER-20-6 #3 in the BULLION forced-gradient experiment on Pahute Mesa, NTS.	LA0302PR831231.003	S03063_001
Solute responses in ER-20-6 #2 in the BULLION forced-gradient experiment on Pahute Mesa, NTS.	LA0302PR831231.002	S03064_001
Breakthrough curves of CML microspheres, silica colloids, and iodide in fractured cores from the NTS.	LA0301PR831352.001	S03034_001
Breakthrough curves of tritium, Pu, and various colloids in fractured cores from borehole UE20c at the NTS.	LA0301PR831361.003	S03026_001
Breakthrough curves of tritium, Pu, and various colloids in fractured cores from boreholes PM-1 and PM-2 at the NTS.	LA0301PR831361.004	S03027_001
RELAP computer code interpretations of solute and microsphere responses in the Bullfrog Tuff and Prow Pass Tuff tracer tests at the C-wells.	LA0303PR831231.003	Model Warehouse Data
Calculations to determine detachment rate constant of microspheres in a singe-well tracer test in saturated alluvium.	LA0303PR831352.001	System Performance Assessment Dataset

Table 3 (Continued). Direct Inputs

Data Description	Data Tracking Number	Data Used
Model interpretations of ER-20-6 field tracer transport experiment	LA0303PR831352.002	Model Warehouse Data
Model interpretations of NTS fractured core colloid and colloid-facilitated transport experiments	LA0303PR831352.003	Model Warehouse Data
RELAP computer code interpretations of laboratory rate constants in alluvium.	LA0303PR831361.001	Model Warehouse Data
Breakthrough curves of CML microspheres, silica colloids, and bromide in alluvium-packed Column A, Run 1.	LA0206MH831361.001	S02152_001
Breakthrough curves of CML microspheres, silica colloids, and bromide in alluvium-packed Column B, Run 1.	LA0206MH831361.002	S02153_001
Breakthrough curves of CML microspheres, silica colloids, and bromide in alluvium-packed Column A, Run 2.	LA0206MH831361.003	S02154_001
Breakthrough curves of CML microspheres, silica colloids, and bromide in alluvium-packed Column B, Run 2.	LA0206MH831361.004	S02155_001
Breakthrough curves of tritium, Pu, and natural colloids in two alluvium-packed columns.	LA0301AA831352.001	S03043_001
Field-scale attachment/detachment rates and retardation factors for colloids in alluvial material*	Technical Information* Schijven et al., 1999 [162423]	Rate constants and retardation factors obtained from model interpretations of colloid breakthrough curves.*

NOTE: *This technical information was obtained from Schijven, J.F., Hoogenboezem, W., Hassanizadeh, S.M., and Peters, J.H. 1999. "Modeling Removal of Bacteriophages MS2 and PRD1 by Dune Recharge at Castricum, Netherlands." *Water Resources Research, 35*, (4), 1101-1111. The information was used because there are no field estimates of colloid-transport parameters in the saturated alluvium south of Yucca Mountain (with the exception of a detachment rate constant obtained in a single-well test at the Alluvium Testing Complex (ATC)). It was desirable to include some field-derived parameter estimates in the colloid-transport parameter distributions for alluvium (e.g., Figure 1). Schijven et al. (1999 [162423], Table 3, p. 1107) measured filtration and detachment rates for bacteriophages in alluvium material under natural gradient conditions. They used bacteriophages denoted as MS-2 and PRD-1 that are in the same size range as colloids. These bacteriophages were chosen because they attach less than most pathogenic viruses and are relatively persistent during transport through the subsurface (Schijven et al. 1999 [162423], p. 1101). Schijven et al. used a modeling approach very similar to RELAP to obtain colloid filtration and detachment rate constants from their field breakthrough curves. The model development and implementation is documented in detail.. The groundwater at the site studied by Schijven et al. (1999 [162423], Table 2, p. 1105) had somewhat higher divalent cation concentrations than most saturated zone (SZ) waters in the vicinity of Yucca Mountain (90-100 mg/L Ca^{2+} and 10-15 mg/L Mg^{2+} compared to 2-20 mg/L Ca^{2+} and 0-5 mg/L Mg^{2+} at Yucca Mountain), so colloids would be expected to be less stable at their site. However, the alluvium material at their study site was also a bit coarser, with more sand, less clay, and more organic carbon than the alluvium material south of Yucca Mountain, all of which would tend to result in enhanced colloid transport relative to Yucca Mountain conditions. Thus, the combination of colloid selection, interpretive method, documentation quality, groundwater chemistry, and alluvium characteristics in the study of Schijven et al (1999 [162423]) suggest it is reasonable to use their reported colloid filtration and detachment rate constants in the development of colloid-transport parameter distributions for Yucca Mountain alluvium.

4.2 CRITERIA

The general requirements to be satisfied by the TSPA are stated in the criteria discussed in Table 4. Technical requirements to be satisfied by the TSPA are identified in the Yucca Mountain Project Requirements Documents (Canori and Leitner 2003 [161770], Table B-4). The acceptance criteria that will be used by the U.S. Nuclear Regulatory Commission (NRC) to determine whether the technical requirements have been met are identified in the *Yucca Mountain Review Plan, Final Report* (YMRP; NRC 2003 [163274]). The pertinent requirements and criteria for this report are summarized in Table 4.

Table 4. Project Requirements and YMRP Acceptance Criteria Applicable to This Scientific Analysis Report

Requirement Number[a]	Requirement Title[a]	10 CFR 63 Link	YMRP Acceptance Criteria[b]
PRD-002/T-014	Performance Objectives for the Geologic Repository After Permanent Closure	10 CFR 63.113	2.2.1.1.3, criteria 1 to 3
PRD-002/T-015	Requirements for Performance Assessment	10 CFR 63.114	2.2.1.3.9.3, criteria 1 to 2
PRD-002/T-016	Requirements for Multiple Barriers	10 CFR 63.115	2.2.1.1.3, criteria 1 to 3

NOTE: [a] from Canori and Leitner (2003 [161770]).
[b] from NRC (2003 [163274]).
[c] from 10 CFR 63 [156605].

Section 2.2.1.1.3 *Acceptance Criteria* [for 2.2.1.1 *System Description and Demonstration of Multiple Barriers*], which are based on meeting the requirements of 10 CFR 63.113(a) and 63.115(a)–(c):

- Acceptance Criterion 1, Identification of Barriers is Adequate:

  Barriers relied on to achieve compliance with 10 CFR 63.113(b), as demonstrated in the total system performance assessment, are adequately identified, and are clearly linked to their capability. The barriers identified include at least one from the engineered system and one from the natural system.

  This analysis report provides information that makes it possible to describe the transport of colloids through the saturated-zone flow system part of the natural system.

- Acceptance Criterion 2, Description of Barrier Capability to Isolate Waste is Acceptable:

  The capability of the identified barriers to prevent or substantially delay the movement of water or radionuclides from the Yucca Mountain Repository is adequately identified and described:

1. The information on the time period over which each barrier performs its intended function, including any changes during the compliance period.

Section 6 of this analysis report develops retardation-factor uncertainty distributions. These distributions are used to predict the transport of radionuclides that sorb onto colloids. The process of colloid transport is, therefore, included in the transport model and is important in evaluating the saturated zone as a barrier for the time scales of interest. The transport model is discussed in the *Site-Scale Saturated Zone Transport* report (BSC 2003 [162419]).

2. The uncertainty associated with barrier capabilities is adequately described in this report.

Specifically, the uncertainties of this report are addressed in Section 7.3.

- Acceptance Criterion 3, Technical Basis for Barrier Capability is Adequately Presented: The technical bases are consistent with the technical basis for the performance assessment.

  Specifically, the retardation-factor uncertainty distributions for colloids developed in Sections 6.4 and 6.5 of this analysis as well as the fraction of colloids that travel unretarded will be used without modification in the TSPA model. The technical basis for assertions of barrier capability is commensurate with the importance of each barrier's capability and the associated uncertainties. The technical bases developed in this analysis to describe the saturated zone natural barrier are commensurate with the importance of the saturated zone as defined in *Risk Information to Support Prioritization of Performance Assessment Models* (BSC 2002 [160780]).

Section 2.2.1.3.9.3 *Acceptance Criteria* [for 2.2.1.3.9 *Radionuclide Transport in the Saturated Zone*], which are based on meeting the requirements of 10 CFR 63.114(a)–(c) and (e)–(g), relating to the radionuclide transport in the saturated zone model abstraction:

- Acceptance Criterion 1, System Description and Model Integration are Adequate:

  2. The description of the aspects of hydrology, geology, geochemistry, design features, physical phenomena, and couplings that may affect radionuclide transport in the saturated zone is adequate.

  In particular, the retardation factor uncertainty distributions developed in this analysis sample a large variability in geochemistry. Therefore, the distributions include this heterogeneity in the geochemical conditions (Section 6.4, 6.5 and 6.6).

  3. The abstraction of radionuclide transport in the saturated zone uses assumptions, technical bases, data, and models that are appropriate and consistent with other related DOE abstractions.

The descriptions and technical bases listed in Sections 6 and 7 provide transparent and traceable support for the abstraction of colloid transport in the saturated zone. The technical bases for the radionuclide transport abstraction is described in the *SZ Flow and Transport Model Abstraction* (BSC 2003 [164870], Section 6), including those issues pertinent to colloid transport. This analysis supports those bases.

4. Boundary and initial conditions used in the abstraction of radionuclide transport in the saturated zone are propagated throughout its abstraction approaches.

For example, the distributions developed in this analysis report are used directly in the abstraction of radionuclide transport in the saturated zone (Sections 6.4, 6.5 and 6.6).

- Acceptance Criterion 2, Data are Sufficient for Model Justification:

1. Geological, hydrological, and geochemical values used in the license application are adequately justified (e.g., retardation factors). Adequate descriptions of how the data were used, interpreted, and appropriately synthesized into the parameters are provided (Sections 6.4, 6.5 and 6.6).

2. Sufficient data have been collected on the characteristics of the natural system to establish initial and boundary conditions for the TSPA abstraction of radionuclide transport in the saturated zone (Sections 6.4, 6.5 and 6.6).

3. Data on the geology, hydrology, and geochemistry of the saturated zone used in the TSPA abstraction are based on appropriate experimental and modeling techniques. These techniques may include laboratory experiments, site-specific field measurements, natural analog research, and process-level modeling studies (Section 6).

4.3 CODES AND STANDARDS

No industrial or technical codes or standards are directly applicable to the scientific analysis described in this report. This report does not directly address any sections or subsections of the Code of Federal Regulations, DOE Orders, and/or other regulatory codes or standards. This activity does not directly support License Application design.

INTENTIONALLY LEFT BLANK

5. ASSUMPTIONS

The underlying assumptions of the colloid transport model are outlined in Table 5 as the first step toward developing the conceptual, mathematical, and computational models needed in PA calculations.

Table 5. Assumptions

No.	Location in this Report	Assumption	Rationale
1.	Section 6.4.3	The cumulative distribution of retardation factors in the volcanics has a lower limit of R=6 (there is zero probability of having a retardation factor less than 6).	This is believed to be a reasonable lower bound for retardation factors experienced by colloids that are reversibly filtered in the volcanics. The fact that smaller retardation factors have been observed in tests is accounted for by estimating a small fraction of colloids moving unretarded through the SZ based on a distribution of observed filtration rate constants. This value is calculated based on existing data (Table 3) so no additional confirmation is necessary.
2.	Section 6.5.3	The cumulative distribution of retardation factors in the alluvium has a lower limit of R = 8 (there is zero probability of having a retardation factor less than 8).	This is believed to be a reasonable lower bound for retardation factors experienced by colloids that are reversibly filtered in the alluvium. The fact that smaller retardation factors have been observed in tests is accounted for by estimating a small fraction of colloids moving unretarded through the SZ based on a distribution of observed filtration rate constants. This value is calculated based on existing data (Table 3) so no additional confirmation is necessary.
3.	Section 6	The combined cumulative distribution of colloid-filtration-rate constants in the SZ can be linearly extrapolated (on a log-log plot) to very low probabilities for the purposes of estimating fractions of colloids transporting unretarded through the SZ.	There are no data available to indicate that this extrapolation is not valid. Such an extrapolation allows the prediction of very small mass fractions of colloids to move unretarded through the SZ, consistent with field observations at DOE sites such as at the ER-20-6 wells at NTS. This extrapolation is derived from existing data (Table 3), so no additional confirmation is necessary.

INTENTIONALLY LEFT BLANK

6. SCIENTIFIC ANALYSIS DISCUSSION

6.1 OBJECTIVES

Colloid retardation is influenced by the attachment and detachment of colloids from immobile surfaces. This analysis demonstrates the development of parameters necessary to estimate attachment and detachment of colloids and, hence, retardation in both fractured tuff and porous alluvium. Field and experimental data specific to fractured tuff are used for the analysis of colloid retardation in fractured tuff. Experimental data specific to colloid transport in alluvial material from Yucca Mountain as well as bacteriophage field studies in alluvial material, which are thought to be good analogs for colloid transport, are used to estimate attachment and detachment of colloids in the alluvial material. There are no alternative scientific approaches or technical methods for calculating these retardation factors.

6.2 FEATURES, EVENTS, AND PROCESSES SUPPORTED BY THIS SCIENTIFIC ANALYSIS

The development of a comprehensive list of features, events, and processes (FEPs) potentially relevant to post-closure performance of the Yucca Mountain repository is an ongoing, iterative process based on site-specific information, design, and regulations. The approach for developing an initial list of FEPs in support of the *Total Systems Performance Assessment for the Site Recommendation (TSPA-SR)* (CRWMS M&O 2000 [153246]) was documented in Freeze et al. (2001 [154365]). The initial FEPs list contained 328 FEPs, of which 176 were included in TSPA-SR models (CRWMS M&O 2000, Tables B-9 through B-17 [153246]). To support the TSPA-LA, the FEPs list was re-evaluated in accordance with the *Enhanced FEP Plan* (BSC 2002, Section 3.2 [158966]). The included FEPs abstractions incorporated in the TSPA-LA model, which is implemented through specific process models or input parameters, are presented as TSPA-LA dispositions. They are specifically addressed in *SZ Flow and Transport Model Abstraction* (BSC 2003, Section 6.2[164870]), *Site-Scale Saturated Zone Flow Model* (BSC 2003, Section 6.2 [162649]), and *Site-Scale Saturated Zone Transport* (BSC 2003, Section 6.2 [162419]). The rationale for excluding a FEP from the TSPA-LA model will be given in the upcoming revision 2 (REV02) of the SZ FEPs report, *Features, Events, and Processes in SZ Flow and Transport* (CRWMS M&O 2001 [153931]). This scientific analysis report does not provide the technical basis for any of the FEPs; however, Table 6 lists the FEPs included in the TSPA-LA that are supported by the results of the analyses described in this document. Details of the implementation of these FEPs are summarized in Section 6.

Table 6. Saturated Zone Included FEPs Supported by the Results in This Scientific Analysis Report

FEP Number and Name	FEP Description	Section	Reference for Full FEP Description
2.2.08.10 .0A Colloidal Transport in the SZ	Radionuclides may be transported in groundwater in the SZ as colloidal species. Types of colloids include true colloids, pseudo colloids, and microbial colloids.	6.3	BSC 2003 [164870], Section 6.2

6.3 COLLOID TRANSPORT PARAMETERS NECESSARY FOR TSPA

Most radionuclides are assumed to sorb onto colloids reversibly (that is, they have measurable desorption rates and can be entirely desorbed from colloids) (BSC 2003 [161620], Section 6.3.3.1). However, Pu and Am can sorb either reversibily or irreversibily onto colloids with the relative percentages of these obtained from an analysis of waste-form degradation and waste-package corrosion processes occurring in the repository near-field environment (BSC 2003 [161620], Section 6.3.3.1). In general, the majority of the Pu and Am sorbed to colloids is irreversibly sorbed, with a typical percentage being 90-99% irreversible and 1-10% reversible (BSC 2003 [161620], Section 6.3.3.2). Irreversibly sorbed Pu and Am are either embedded in waste-form colloids (e.g., smectite colloids formed by degradation of high-level waste glass) or are so strongly sorbed onto colloids (e.g., iron oxyhydroxide colloids formed by corrosion of waste packages) that there is no possibility of detachment for typical transport time scales (thousands of years) through the SZ. Note that the *EBS Radionuclide Transport Abstraction* (BSC 2003 [163935]), specifically Attachment II discusses the mathematical implementation for irreversible sorption of Pu and Am onto iron oxyhydroxide colloids in the EBS.

By definition, the irreversibly sorbed Pu and Am transport in a manner identical to the colloids onto which they are sorbed. Therefore, the colloid retardation factor uncertainty distributions developed in this analysis are necessary to describe the transport of the irreversibly sorbed radionuclides. Several field observations have suggested that a small percentage of colloids transport with essentially no retardation in groundwater (Kersting et al. 1999 [103282], p. 56; Penrose et al. 1990 [100811], p. 228), whereas the majority undergoes either reversible or irreversible filtration, which can be described by a retardation factor, R_{col}. The value of R_{col} is dependent on several factors such as colloid size, colloid type, and geochemical conditions (e.g., pH, Eh, and ionic strength). These factors are folded into the distribution of R_{col} that has been developed from field and experimental data collected under varying geochemical conditions with different colloid types and sizes. Attachment rate constants, k_{att}, and detachment rate constants, k_{det}, of colloids to the rock matrix have been measured, and separate R_{col} uncertainty distributions have been developed for the fractured volcanics and the alluvium.

The attachment rate constant [T^{-1}] is also used to determine the fraction, *colfrac*, of the colloids that transport with no retardation. Specifically, the inverse of the attachment rate constant

provides a measure of the reaction timescale. Colloids for which this reaction timescale is smaller than the travel time through the system will transport with no retardation. The following sections document the development of R_{col} uncertainty distributions for the volcanics and the alluvium as well as the fraction of colloids that transport unretarded, *colfrac*.

6.4 COLLOID TRANSPORT IN FRACTURED TUFF

6.4.1 Background

Colloid filtration rate constants and retardation factors for the fractured volcanics have been estimated in a number of laboratory and field experiments conducted for the YMP and the Underground Test Area Project. All of the field measurements have involved fluorescent carboxylate modified polystyrene latex (CML) microspheres ranging in size from 280- to 830-nm diameter. Laboratory fracture experiments have been conducted using silica, montmorillonite, and clinoptilolite colloids in addition to CML microspheres. In one study, silica colloid transport (~100-nm diameter) was compared directly with CML microsphere transport (330-nm diameter), and it was found that the microspheres transported conservatively relative to the silica colloids (Anghel 2001 [158639], Chapter 6). This result suggests that colloid filtration and retardation parameters derived from CML microsphere responses in field tracer tests should be conservative if used to predict natural inorganic colloid transport in fractured systems.

Colloid filtration and detachment rate constants have been derived from colloid responses in tracer tests by using the advection-dispersion equation (Freeze and Cherry [101173], p. 389, Equation 9.3) with appropriate terms for a single reversible first-order reaction to account for mass transfer between mobile water and immobile surfaces (filtration and detachment) to fit the data:

$$\frac{\partial C}{\partial t} + V\frac{\partial C}{\partial x} - D\frac{\partial^2 C}{\partial x^2} - k_{filt}C - k_{\det}S = 0 \qquad \text{(Eq. 1)}$$

$$\frac{\partial S}{\partial t} - k_{filt}C + k_{\det}S = 0 \qquad \text{(Eq. 2)}$$

where

C = colloid concentration in solution, no./cm^3

S = no. of colloids attached to fracture surfaces per unit volume of solution, no./cm^3

V = flow velocity in fractures, cm/sec

D = dispersion coefficient, cm^2/sec

k_{filt} = filtration rate constant (1/sec) = λV, where λ = filtration coefficient (1/cm). Note that $k_{filt} = k_{att}$ for the remainder of this document.

k_{det} = detachment rate constant, 1/sec

x, t = independent variables for distance and time, respectively.

Equations 1 and 2 can be solved semi-analytically using the RELAP computer code, which has been used extensively in the Yucca Mountain Project to interpret laboratory- and field-scale tracer tests in single- or dual-porosity media (e.g., upcoming model report ANL-NBS-HS-000039, BSC 2003 [162415]). The procedure for determining colloid filtration and detachment rate constants, k_{filt} and k_{det}, from laboratory or field transport experiments is:

1. Nonsorbing solute tracers were always injected simultaneously with the colloid tracer(s). The mean residence time (L/V, where L = travel distance) and dispersivity (D/V) in the flow system were determined using RELAP to fit the solute breakthrough curves using Equation 1 with k_{filt} and k_{det} set to zero. In dual-porosity systems, diffusive mass-transfer parameters were also estimated for the solutes (upcoming model report ANL-NBS-HS-000039, BSC 2003 [162415], Section 6), so that the effects of diffusion and dispersion could be distinguished and separately accounted for in the flow system(s). Diffusive mass-transfer parameters were determined by simultaneously fitting the responses of two nonsorbing tracers with different diffusion coefficients or of the same nonsorbing tracer at different flow rates through the system(s). In field tests, because of the low tracer recovery in many cases, the fraction of tracer mass participating in the test was allowed to be an additional adjustable parameter for fitting the solute breakthrough curves. The best-fitting fraction for solutes was then applied to the colloids with the rationale that the flow pathways resulting in incomplete recovery of solutes would affect the simultaneously injected colloids similarly.

2. The mean residence time, dispersivity, and mass fraction (in the case of field tests) obtained from fitting the solute breakthrough curves were assumed to apply to the colloids in each experiment. However, on rare occasions, it was necessary to adjust the dispersivity slightly in laboratory experiments to account for a greater apparent dispersion of the colloids (generally because of an earlier first arrival time of the colloids).

3. RELAP was used to fit the colloid breakthrough curves by adjusting k_{filt} and k_{det} (and fixing the mean residence time, dispersivity, and mass fraction to be that of the solutes). The procedure actually involved adjusting the colloid retardation factor, R_{col}, and k_{filt}. k_{det} was then calculated by rearrangement of the relationship (Freeze and Cherry [101173], p. 404, Equation 9.14).

$$R_{col} = 1 + \frac{k_{filt}}{k_{\mathrm{det}}} \qquad \text{(Eq. 3)}$$

4. R_{col} (and, hence, k_{det}) was constrained primarily by fitting the tails of the colloid breakthrough curves. k_{filt} was constrained primarily by fitting the early (unretarded) colloid response (i.e., the peak arriving at about the same time as nonsorbing solutes). Essentially, k_{filt} was adjusted until it was small enough that the fraction of colloids NOT filtered within the system matched the early arriving peak. Thus, the early colloid response was implicitly interpreted as being a fraction of colloids that moved through the system without ever becoming filtered. Similarly, R_{col} was adjusted until an appropriate fraction of filtered colloids was predicted to detach and appear as the tails of the colloid breakthrough curves.

5. In tests in which there was an inadvertent flow transient that resulted in a “spike” in colloid concentrations in the tail of the breakthrough curve (presumably because of enhanced

detachment caused by the flow transient), the value obtained for R_{col} (and k_{det}) was not considered to be representative of steady-flow conditions. However, the value obtained for k_{filt}, which was constrained primarily by the colloid response occurring before the flow transient, was assumed to be representative of steady-flow conditions. Thus, k_{filt} values obtained from such tests were used in the development of cumulative distribution functions (CDFs) for filtration rate constants, but R_{col} values from these tests were not used in the development of CDFs for retardation factors.

6.4.2 Colloid Filtration Rate Constants for Fractured Volcanics

Figure 1 shows a plot of filtration rate constants obtained from interpretations of several field and laboratory tracer tests conducted in saturated fractured rocks as a function of the time to reach peak nonsorbing solute concentrations in the tests. The filtration rate constants reflect the fraction of colloids that were not filtered during the tests (i.e., the rate constant is constrained primarily by the magnitude of the early arrival of colloids). Figure 1 also shows that, even though different sizes and types of colloids were used in the different tests, there is an apparent trend of decreasing filtration rate constant with residence time. The line drawn through the data (not a fit) has a slope of –1 in log space, which implies an inverse time dependence of the filtration rate constant. Schijven et al. (1999 [162423], Table 3, p. 1107) observed a similar decrease in filtration rate constants as a function of distance (proportional to time in their system) for bacteriophage transport in a sandy alluvial aquifer.

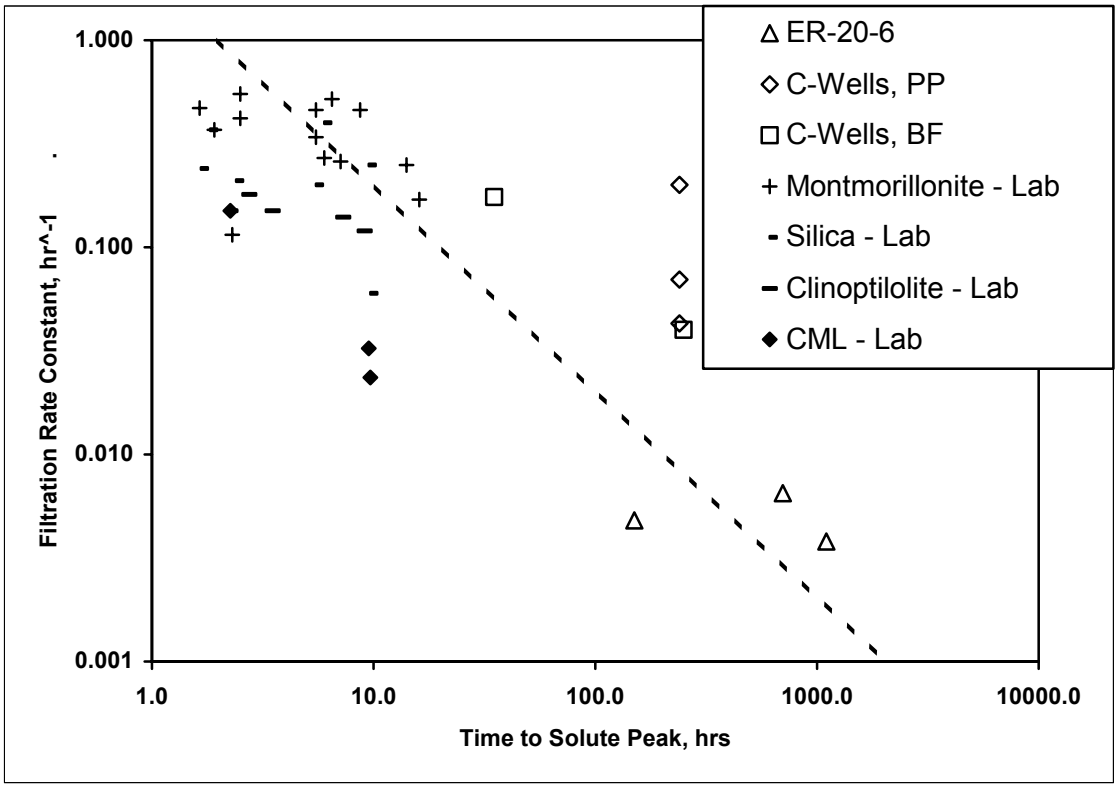

DTN: LA0007PR831231.001 (C-Wells BF data);
LAPR831231AQ99.001 (C-Wells PP data);

LA0302PR831352.002 (ER-20-6 well 3 data);
LA0302PR831352.001 (ER-20-6 well 2 data);
LA0302PR831231.003 (ER-20-6 well 3 solute data);
LA0302PR831231.002 (ER-20-6 well 2 solute data);
LA0301PR831352.001 (silica and CML data);
LA0301PR831361.003 (silica and montmorillonite data);
LA0301PR831361.004 (montmorillonite and clinoptilolite data);
LA0303PR831231.003 (analysis of C-wells rate constants);
LA0303PR831352.002 (analysis of ER-20-6 rate constants);
LA0303PR831352.003 (analysis of laboratory rate constants).

NOTE: "ER-20-6" refers to the BULLION forced-gradient experiment (Reimus and Haga 1999 [154705], p. 1). "C-wells BF" and "C-wells PP" refer to tests in the Bullfrog Tuff and Prow Pass Tuff (both members of the Crater Flat Group), respectively, at the UE-25 C-wells (BSC 2003 [162415], Section 6). The lab experiments were all conducted in the laboratory using fractured cores from Pahute Mesa at NTS. It is important to emphasize that different CML microspheres were used in the different field tests and, also, the groundwater chemistry varied from site to site or test to test. The dashed line on the figure has a slope of –1in log space.

Figure 1. CML Microsphere and Inorganic Colloid Filtration Rate Constants as a Function of Time to Solute Peak Concentration in Several Field and Laboratory Tracer Tests in Saturated, Fractured Media

The trend shown in Figure 1 suggests that some fraction of colloids may always transport through a fracture flow system regardless of the time or length scale of the observations. It is tempting to draw the conclusion that filtration rate constants will continually decrease with increasing time scales. However, it may be more appropriate to consider the possibility that, while the majority of colloids might be filtered quite quickly, there is a small fraction that are resistant to filtration and, therefore, capable of traveling large distances over long time periods. This statement implies that there may be a distribution of colloid filtration rate constants rather than a fixed rate constant that applies to all colloids. The appearance of a small fraction of colloids at about the same time as nonsorbing solutes in tracer tests, regardless of the overall time scale of the test, forces filtration rate constants to decrease with time when single rate constants are assumed to apply to all colloids.

Ignoring the possible scale effect for the moment, it is possible to construct a CDF for the filtration rate constants derived from all of the experiments represented in Figure 1. In doing so, filtration rate constants derived from field tests were weighted to be twice that of rate constants from laboratory tests, as tests at field scales are considered more relevant to TSPA modeling. The weighting factor was chosen using professional judgment. Also, one data point was added that does not come from a tracer test but rather from the observation(s) of colloid-facilitated Pu transport in the ER-20-5 wells that originated from the BENHAM nuclear test cavity (Kersting et al. 1999 [103282], pp. 56-59). To estimate a filtration rate constant for this observation, the following several assumptions were made:

- The Pu in the ER-20-5 wells was irreversibly sorbed to colloids, which means that Pu concentrations in the wells reflect the colloid transport parameters.

- The concentrations measured in ER-20-5 #1 (on the order of 10^{-13} M Pu) represent a five order-of-magnitude decrease from concentrations at the source. Thus, colloid filtration is assumed to result in a five order-of-magnitude decrease in colloid concentrations.

- Any colloids that were filtered would never make it to the observation wells (i.e., they were effectively irreversibly filtered).

- The travel time from the source to the ER-20-5 wells was ~30 years, which represents an upper-bound estimate. Note that we define travel time as the 50%-ile concentration breakthrough.

No assumptions were required about the travel distance. Although these assumptions cannot be verified directly, they allow us to estimate a filtration rate constant using the following expression:

$$1\times10^{-5} = \mathrm{Exp}[-(30)(365.25)(24)k_{filt}] \qquad \text{(Eq. 4)}$$

where

1×10^{-5} = fraction of colloids traveling from the source to the ER-20-5 wells

(30)(365.25)(24) = 262,980 = travel time in hours.

Note that Equation 4 is obtained from Equation 2 for a batch system in which there are no advection and dispersion terms. In addition, the detachment rate, k_{det}, is zero as well, yielding Equation 4.

Solving Equation 4 for k_{filt} yields a filtration rate constant of 4.4×10^{-5} hr^{-1}. This estimate is not very sensitive to the fraction of colloids assumed on the left-hand side of Equation 4. If the fraction is changed to 1×10^{-8}, the filtration rate constant becomes 7×10^{-5} hr^{-1}. The filtration rate constant is inversely proportional to the assumed travel time; consequently, if the travel time is decreased by a factor of 3 to 10 years, the filtration rate constant increases by a factor of 3 to 1.3×10^{-4} hr^{-1}.

Figure 2 shows the resulting cumulative probability distribution of filtration rate constants that includes the data point corresponding to the ER-20-5 observations (which was weighted the same as the field tracer test results). Both axes in Figure 2 are logarithmic. Note that data points associated with the two alternative assumptions discussed above for the ER-20-5 observations are also shown in Figure 2 (as squares) to illustrate the insensitivity of the overall cumulative distribution to these assumptions. However, these points are not used in the fit.

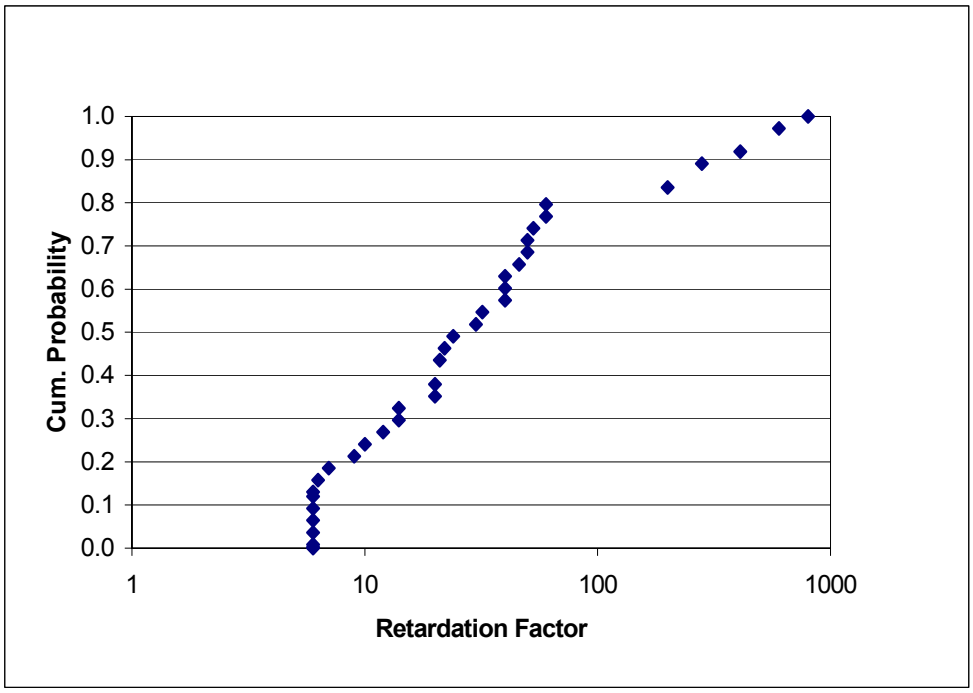

Source: Notebook SN-LANL-SCI-297-V1 (Viswanathan 2003 [163757], p 11)

NOTE: The two squares show the effect of changing the assumptions associated with the filtration rate constant estimates for the ER-20-5 observations (see text).

Figure 2. Cumulative Probability Distribution of Log Colloid Filtration Rate Constants for Fractured Media

6.4.3 Colloid Retardation Factors for Fractured Volcanics

Using the interpretive results from all the tests represented in Figure 2, with the exception of the ER-20-5 observations and two of the three CML microsphere responses from the BULLION forced-gradient experiment (Reimus and Haga 1999 [154705], pp. 29-31, Figures 13-15), a cumulative probability distribution for R_{col} can be generated. This distribution is shown in Table 7 and Figure 3 (log scale on x axis), which again has the field test results weighted a factor of two greater than the laboratory test results. Table 7 contains three cumulative probability distributions. The first distribution consists of the best-fitting R_{col} values obtained from RELAP (taken from the input DTNs listed in Figure 1). The second distribution is a truncated version of this CDF in which all retardation factors less than 6 are set equal to 6. The final distribution is the CDF for use by TSPA, which captures the same trends as the truncated CDF while using fewer points. The CDF for TSPA represents the uncertainty in the retardation factor for colloids in the volcanic units. These values of retardation factors in the CDF can be applied on a log scale for the purposes of TSPA. The rationale for truncating the original CDF at $R_{col} = 6$ is that 6 is the smallest value of R_{col} that is reasonably well constrained by fitting the tails of colloid breakthrough curves. R_{col} values less than 6 were poorly constrained because the breakthrough curves had relatively high recoveries and tails with low concentrations that could be fitted quite well over a wide range of R_{col} values (the fits were much more sensitive to k_{filt} than R_{col}). In the extreme case of tests with nearly complete colloid recoveries and low tail concentrations, the breakthrough curves could be fit equally well with $R_{col} = 1$ and k_{filt} = anything or with R_{col} = a very large number and k_{filt} = a very small number. In either case, the implication is that there is no filtration, and the test data, in effect, provide no constraint whatsoever on R_{col} or k_{filt}. In these situations, RELAP would default to a best fit with $R_{col} = \sim 1$. R_{col} values greater than 1 but less than 6 were poorly constrained because they were associated with fits that were relatively insensitive to values of R_{col} and k_{filt}, although some combination of a low value of R_{col} and an intermediate value of k_{filt} offered the best least-squares fit.

The ER-20-5 observations were omitted from the R_{col} distribution(s) because it was assumed that k_{det} was zero when estimating k_{filt} (i.e., R_{col} = infinite). Also, the results from the two microsphere responses in the BULLION forced-gradient experiment production well were omitted because there was a significant increase in microsphere concentrations in the tails of the responses that apparently resulted from a flow transient in the production well. This increase prevented an unbiased estimate of k_{det}. The maximum retardation factor assumed for any of the colloid data sets was 1000. For any of these data sets, the factor of 1000 could effectively not be distinguished from an infinite retardation factor (R_{col} values greater than a few hundred in most cases were equivalent to assuming irreversible filtration, or R_{col} = infinite). Thus, the distribution of Figure 2 is probably conservative at the high end because of this somewhat arbitrary maximum value.

Table 7. Retardation Factor, R_{col}, Cumulative Probability Distributions for Fractured Volcanics

Raw Data CDF		Truncated CDF		CDF for TSPA	
Retardation Factor	Cumulative Probability	Retardation Factor	Cumulative Probability	Retardation Factor	Cumulative Probability
1	0.00001	6	0.00001	6.00	0
1.162	0.001942	6	0.001942	6.00	0.15
1.19	0.008424	6	0.008424	10.23	0.25
2	0.036202	6	0.036202	26.00	0.5
2.5	0.063979	6	0.063979	59.98	0.8
2.5	0.091757	6	0.091757	800.00	1
3.25	0.119535	6	0.119535		
3.5	0.147313	6	0.12972		
6.3	0.157498	6.3	0.157498		
7	0.185276	7	0.185276		
9	0.213053	9	0.213053		
10	0.240831	10	0.240831		
12	0.268609	12	0.268609		
14	0.296387	14	0.296387		
14	0.324165	14	0.324165		
20	0.351942	20	0.351942		
20	0.37972	20	0.37972		
21	0.407498	21	0.435276		
22	0.463053	22	0.463053		
24	0.490831	24	0.490831		
30	0.518609	30	0.518609		
32	0.546387	32	0.546387		
40	0.574165	40	0.574165		
40	0.601942	40	0.601942		
40	0.62972	40	0.62972		
46	0.657498	46	0.657498		
50	0.685276	50	0.685276		
50	0.713053	50	0.713053		
53	0.740831	53	0.740831		
60	0.768609	60	0.768609		
60	0.796387	60	0.796387		
200	0.835276	200	0.835276		
280	0.890831	280	0.890831		
410	0.918609	410	0.918609		
600	0.946387	600	0.946387		
800	1	800	1		

Output DTN: LA0303HV831352.002.

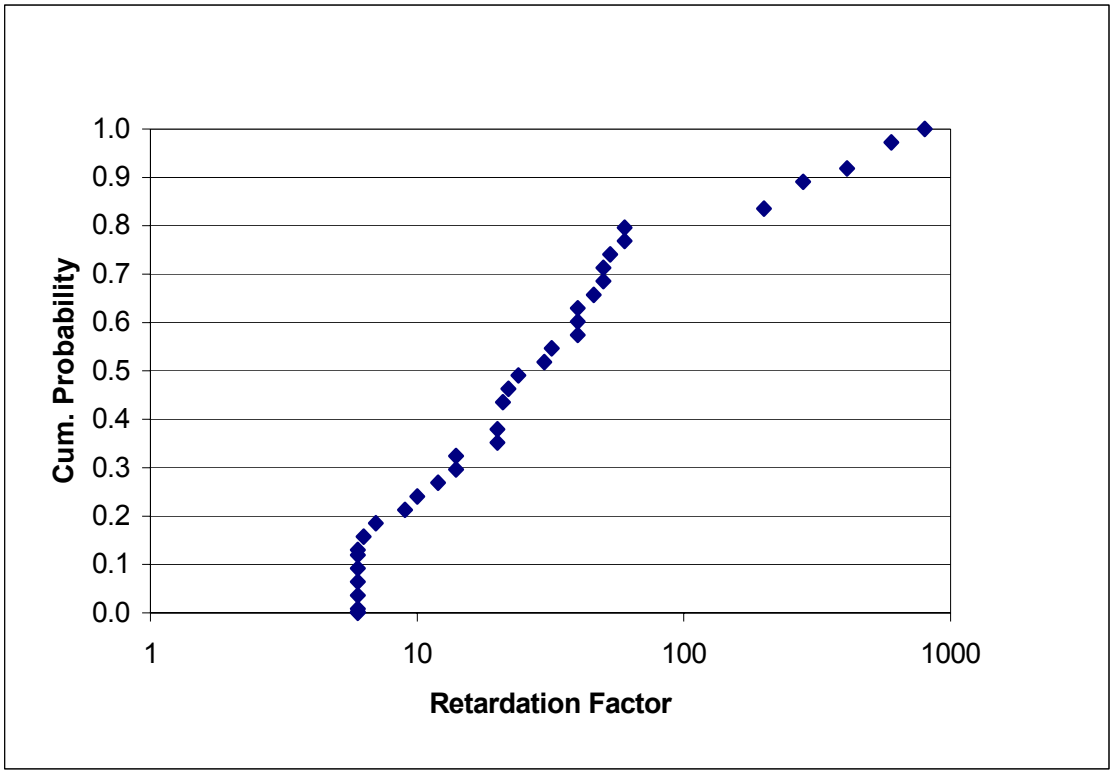

Source: Notebook SN-LANL-SCI-297-V1 (Viswanathan 2003 [163757], p. 23)

NOTE: See text for recommendations on how to use the fits to generate stochastic retardation factors.

Figure 3. Truncated Cumulative Probability Distribution of Retardation Factors for the Fractured Volcanics

Figure 3 shows a fit to the cumulative distribution for retardation factors using the truncated data shown in Table 7. Note that the cumulative distribution of retardation factors in the volcanics has a lower limit of $R_{col} = 6$ (there is zero probability of having a retardation factor less than 6). This is believed to be a reasonable lower bound for retardation factors experienced by colloids that are reversibly filtered in the volcanics. The fact that smaller retardation factors have been observed in tests is attributed to slow filtration rate constants that result in a fraction of the colloids moving conservatively through flow systems. The approach advocated here is to account for this unretarded fraction of colloids using a distribution of observed filtration rate constants, with unretarded colloids having the slowest rates. It is then assumed that all colloids that become filtered experience some minimum delay in the system as a result of filtration and detachment processes. This minimum delay in the fractured volcanics corresponds to a retardation factor of 6.

6.5 COLLOID TRANSPORT IN ALLUVIAL MATERIAL

6.5.1 Background

Colloid filtration rate constants and retardation factors for alluvial material have been estimated in a number of laboratory experiments for the YMP. With the absence of YMP field data for colloid filtration in the alluvium, data from Schijven et al. (1999 [162423], Table 3, p. 1107) were used to obtain field colloid filtration and detachment rates.

Laboratory column experiments have been conducted using silica and natural colloids in addition to CML microspheres.

Schijven et al. (1999 [162423], Table 3, p. 1107) measured filtration and detachment rates for bacteriophages in alluvial material under natural gradient conditions. They used bacteriophages denoted as MS-2 and PRD-1 that are in the same size range as colloids. These bacteriophages were chosen because they attach less than most pathogenic viruses and are relatively persistent during transport through the subsurface (Schijven et al. 1999 [162423], p. 1101). The groundwater at the site studied by Schijven et al. (1999 [162423], Table 2, p. 1105) had somewhat higher divalent cation concentrations than most SZ waters in the vicinity of Yucca Mountain (90-100 mg/L Ca^{2+} and 10-15 mg/L Mg^{2+} compared to 2-20 mg/L Ca^{2+} and 0-5 mg/L Mg^{2+} at Yucca Mountain), so colloids would be expected to be less stable at their site. However, the alluvium material at their study site was also a bit coarser, with more sand, less clay, and more organic carbon than the alluvium material south of Yucca Mountain, all of which would tend to result in enhanced colloid transport relative to Yucca Mountain conditions. Thus, the combination of colloid selection, groundwater chemistry, and alluvium characteristics at the site studied by Schijven et al (1999 [162423]) suggest that there are no obvious reasons why their reported colloid filtration and detachment rate constants cannot be applied to Yucca Mountain alluvium (as long as it is recognized that there are uncertainties associated with doing so).

As with the fractured volcanics, colloid filtration and detachment rate constants have been derived from colloid responses in tracer tests by using the advection-dispersion equation with appropriate terms for a single reversible first-order reaction to account for mass transfer between mobile water and immobile surfaces (filtration and detachment) to fit the data. Equations 1, 2, and 4 also apply to colloid filtration in the alluvium.

As was the case for the fractured volcanics, the values for V and D in Equations 1 and 2 were always obtained from interpretations of nonsorbing solute tracer responses; therefore, the filtration and detachment rate constants were the only parameters adjusted to match the colloid breakthrough curves.

6.5.2 Colloid Filtration Rate Constants in Alluvial Material

Figure 4 shows a plot of filtration rate constants obtained from interpretations of several laboratory tracer tests and the Schijven et al. (1999 [162423], Table 3, p. 1107) field test conducted in saturated alluvium as a function of the mean solute residence time in the tests. The filtration rate constants reflect the fraction of colloids that were not filtered during the tests (i.e., the rate constant is constrained primarily by the magnitude of the early arrival of colloids).

Figure 4 also shows that, even though different sizes and types of colloids were used in the different tests, there is an apparent trend of decreasing filtration rate constant with residence time. This trend is similar to the trend witnessed in the fractured volcanics. However, the experiments involving the two colloids with the largest filtration rate constants, the 330-nm CML microspheres and the 100-nm silica colloids, were conducted in columns in which air bubbles became apparent during the experiments. Later alluvium column experiments that involved the 190-nm and 500-nm CML microspheres, as well as the natural colloids, were conducted much more carefully to avoid air bubbles. It is certainly possible that the air bubbles in the earlier tests could have been at least partly responsible for the greater filtration rate constants in these tests. Figure 5 shows the resulting cumulative probability distribution of filtration rate constants in the alluvium.

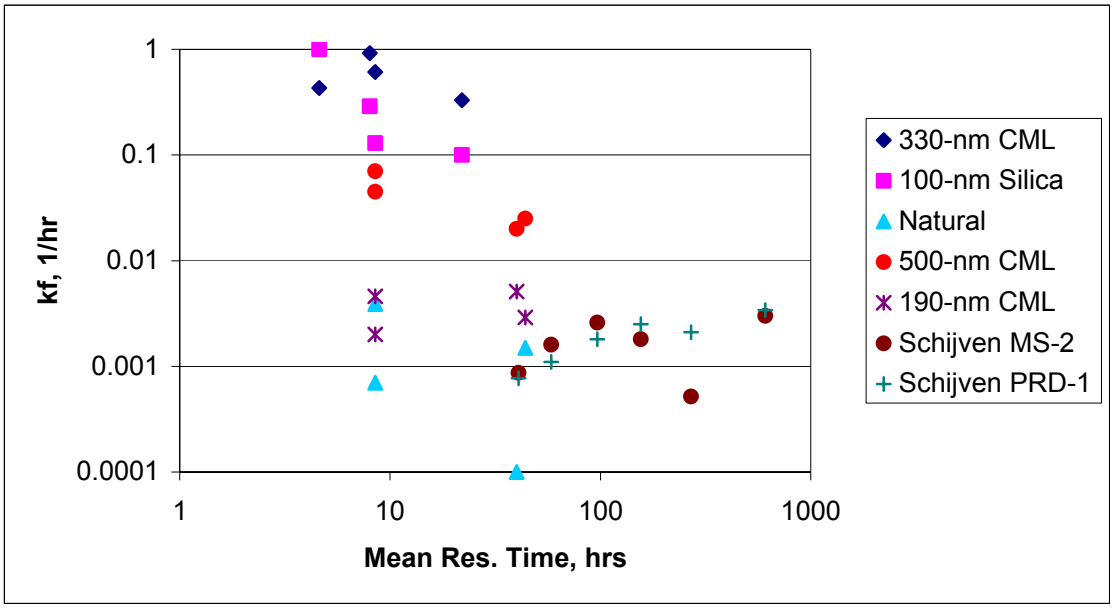

DTN: LA0206MH831361.001 (330-nm CML and 100-nm silica data);
LA0206MH831361.002 (330-nm CML and 100-nm silica data);
LA0206MH831361.003 (330-nm CML and 100-nm silica data);
LA0206MH831361.004 (330-nm CML and 100-nm silica data);
LA0301AA831352.001 (500-nm CML, 190-nm CML and natural colloids data);
LA0303PR831361.001 (Analysis of all laboratory rate constants);
Schijven et al. 1999 [162423] (MS-2 and PRD-1 rate constants from alluvium field test)

NOTE: CML, Silica and Natural Colloids are rate constants obtained from alluvium packed columns and Schijven MS-2 and Schijven PRD-1 are rate constants from the alluvium field test.

Figure 4. Colloid Filtration Rate Constants as a Function of Mean Residence Time in Several Laboratory Experiments and a Field Study in Saturated, Alluvium Material

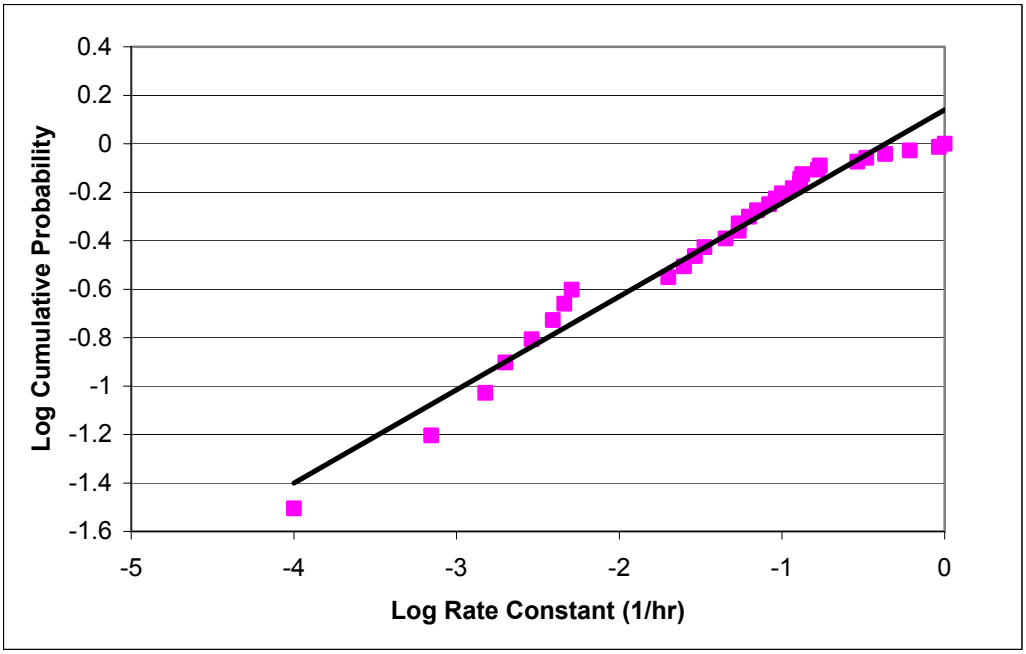

Source: Notebook SN-LANL-SCI-297-V1 (Viswanathan 2003 [163757], p. 20).

Figure 5. Cumulative Probability Distribution of Log Colloid Filtration Rate Constants in the Alluvium

6.5.3 Colloid Retardation Factors in Alluvial Material

As with the fractured volcanics, colloid retardation factors, R_{col}, can be calculated from colloid filtration and detachment rate constants using Equation 3. Using the interpretive results from all of the tests represented in Figure 3, a cumulative probability distribution for R_{col} can be generated. This distribution is shown in Table 8 and Figure 6 (log scale on x axis). Table 8 contains three cumulative probability distributions. The first distribution consists of the best-fitting R_{col} values obtained from RELAP (taken from the input DTNs listed in Figure 4). The CDF for TSPA represents the uncertainty in the retardation factor for colloids in the alluvium. These values of retardation factors in the CDF can be applied on a log scale for the purposes of TSPA. The second distribution is a truncated version of this CDF in which all retardation factors less than 8 are set equal to 8. This truncation was implemented for the same reasons that the R_{col} distribution for fractured volcanics was truncated (see Section 6.4.3). The final distribution is the CDF for use by TSPA to simulate radionuclide retardation for the radionuclides that sorb irreversibly to colloids, which captures the same trends as the truncated CDF while using fewer points. Note that the filtration rate constants and retardation factors from Schijven et al. (1999 [162423], Table 3, pg. 1107) are weighted the same as all lab experimental data when generating uncertainty distributions of filtration rate constants and retardation factors in the alluvium. Although the Schijven et al. data were obtained at field scales, the fact that the flow system and aquifer materials are different from Yucca Mountain justifies assigning no greater weight to these data than to data obtained from lab experiments using site-specific materials. Note that, as with the retardation factor distribution for the fractured volcanics, the alluvium retardation factor

distribution is truncated at the lower end so that it has an effective minimum greater than one; in this case, the minimum is eight. The rationale for this minimum is the same as for the volcanics: that is, the colloids moving with smaller retardation factors are accounted for using a distribution of filtration rate constants, with unretarded colloids having the slowest rates; all colloids that become filtered experience some degree of retardation in the system as a result of filtration and detachment processes.

Table 8. Retardation Factor, R_{col}, Cumulative Probability Distributions for Alluvium

Raw Data CDF		Truncated CDF		CDF for TSPA	
Retardation Factor	Probability	Retardation Factor	Probability	Retardation Factor	Probability
1	0.03125	8	0.03125	8.00	0
1	0.0625	8	0.0625	8.00	0.331
1	0.09375	8	0.09375	33.96	0.5
1.5	0.125	8	0.125	5188.00	1
1.5	0.15625	8	0.15625		
1.5	0.1875	8	0.1875		
1.5	0.21875	8	0.21875		
1.5	0.25	8	0.25		
4.5	0.28125	8	0.28125		
8	0.3125	8	0.3125		
14	0.34375	14	0.34375		
16	0.375	16	0.375		
17	0.40625	17	0.40625		
20	0.4375	20	0.4375		
26	0.46875	26	0.46875		
34	0.5	34	0.5		
35	0.53125	35	0.53125		
55	0.5625	55	0.5625		
140	0.59375	140	0.59375		
160	0.625	160	0.625		
205.8824	0.65625	205.8824	0.65625		
266.6667	0.6875	266.6667	0.6875		
600	0.71875	600	0.71875		
619.0476	0.75	619.0476	0.75		
1076.923	0.78125	1076.923	0.78125		
1111.111	0.8125	1111.111	0.8125		
1222.222	0.84375	1222.222	0.84375		
2000	0.875	2000	0.875		
2500	0.90625	2500	0.90625		
2818.182	0.9375	2818.182	0.9375		
4712.644	0.96875	4712.644	0.96875		
5194.805	1	5194.805	1		

Output DTN: LA0303HV831352.004.

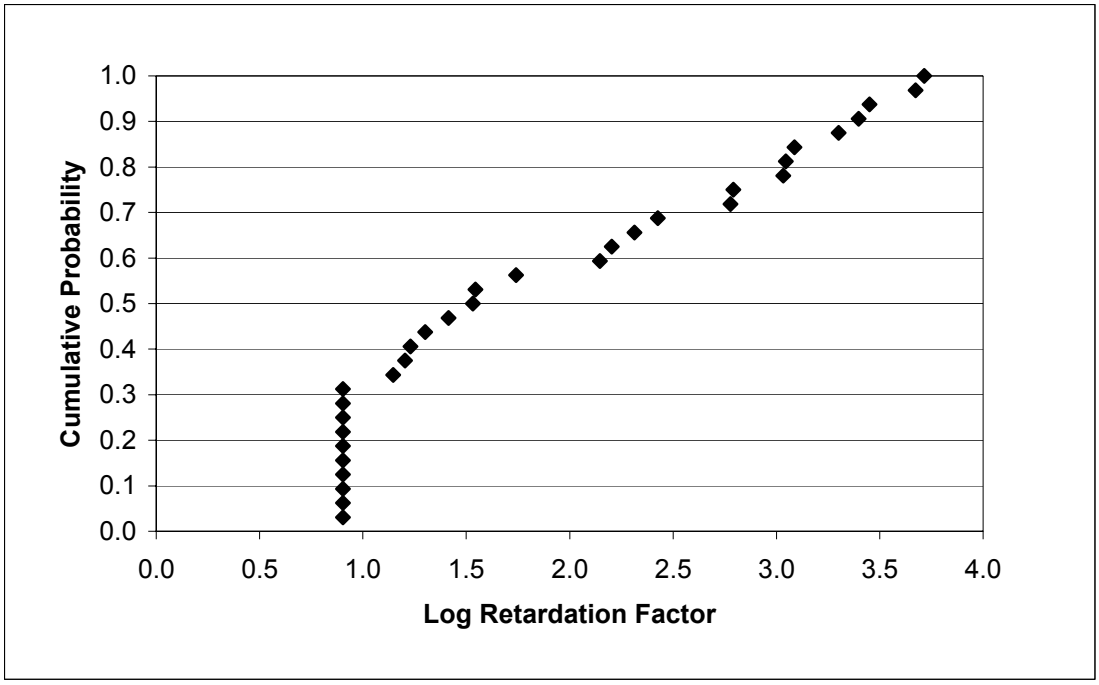

Source: Notebook SN-LANL-SCI-297-V1 (Viswanathan 2003 [163757], p. 24).

Figure 6. Truncated Cumulative Probability Distribution of Log Retardation Factors in Alluvium

6.6 FRACTION OF COLLOIDS TRANSPORTING WITH NO RETARDATION

The majority of the colloids transport assuming reversible filtration given by the *Rcol* distributions developed in Sections 6.4.3 and 6.5.3. However, as mentioned in Section 6.3, several field observations have suggested that a small percentage of colloids transport with essentially no retardation in groundwater, whereas the majority undergoes either reversible or irreversible filtration, which can be described by a retardation factor, R_{col}. In this section, the cumulative probability distribution of colloids that travel with no retardation is developed.

The attachment rate constant can be used to determine the fraction, *colfrac*, of the colloids that transport with no retardation. Specifically, colloids for which the reciprocal of the attachment rate constant is smaller than the travel time through the system will transport with no retardation. To determine the fraction of colloids that travel with no retardation, the critical rate constant, $k_{filt,crit}$ is calculated. This critical rate constant is simply one over the travel time through the system. The fraction of colloids that filter with this attachment rate constant is obtained from the cumulative probability distribution of attachment constants (Figure 2 for the fractured volcanics and Figure 5 for the alluvium). For the distribution of unretarded colloid fractions, water travel times through the UZ (which will include the effects of hydrologic fracture-matrix interactions), the SZ volcanics (in fractures only), and the SZ alluvium are added to obtain a combined travel time from the waste package to the accessible environment. Because the distributions for the fraction unretarded are so close for the volcanics and the alluvium, the volcanic and alluvium

data are combined into a single distribution, resulting in slightly higher fractions for a given travel time than if the volcanic and alluvium uncertainty distributions had been considered separately.

The TSPA model utilizes the fast fraction model in the following manner. Travel time is uncertain through both the UZ and SZ, and the fast fraction model is also uncertain. Therefore experimental evidence for this model does not warrant the use of a travel time distribution in TSPA. Instead, a conservative model is implemented. Since it is highly unlikely that any TSPA realization will have a combined UZ-SZ travel time of less than 100 years, TSPA uses the fast fraction value corresponding to 100 years from the combined curve.

Table 9 and Figure 7 show the distribution of the fraction of colloids that travel with no retardation. For example, in each TSPA realization of the saturated-zone transport model in which the travel time is 100 years, the fraction of the total colloid mass transporting with no retardation would be 0.001678.

Table 9. Unretarded Fraction Cumulative Probability Distribution for the Fractured Volcanics and the Alluvium

Travel Time (Years)	Unretarded Fraction, colfrac
1	0.011
5	0.005702
10	0.004297
20	0.003238
30	0.002744
40	0.00244
50	0.002227
75	0.001888
100	0.001678
300	0.001072
600	0.000808
1000	0.000656
2000	0.000494
5000	0.00034
10000	0.000256

Output DTN: LA0303HV831352.003.

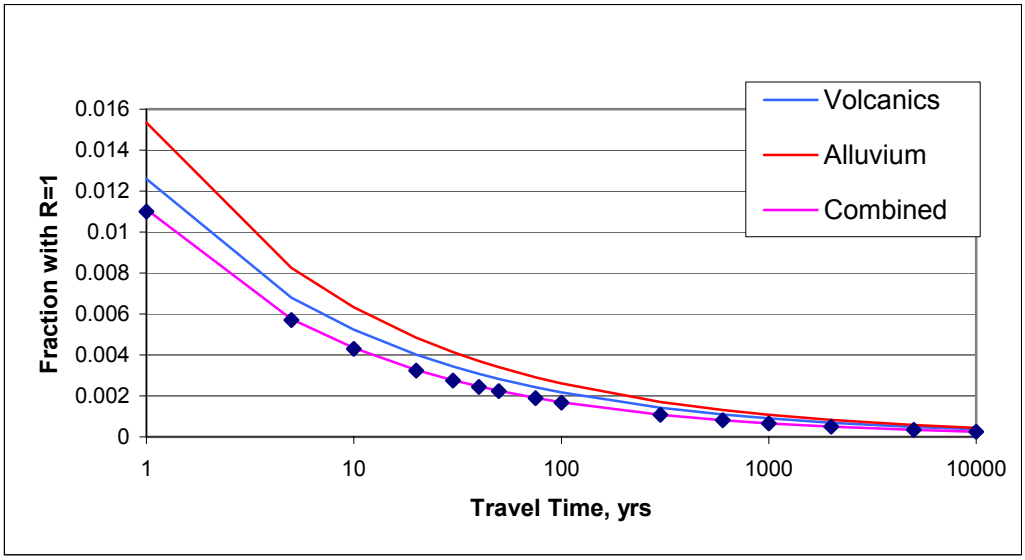

Source: Notebook SN-LANL-SCI-297-V1 (Viswanathan 2003, p. 22).

Figure 7. Unretarded Fraction Cumulative Probability Distribution for the Fractured Volcanics, Alluvium, and the Combined Distribution of the Volcanics and Alluvium

6.7 THE VALIDITY OF THE LOCAL EQUILIBRIUM ASSUMPTION FOR COLLOIDS THAT ARE RETARDED

The majority fraction of colloids is retarded by the R_{col} uncertainty distributions developed in this analysis. The validity of the local equilibrium assumption must be tested to justify the use of the R_{col} distributions. Specifically, for Equation 3 to be valid, the local equilibrium assumption must hold. To evaluate the validity of this assumption, a simple analysis can be performed with nondimensional Damköhler numbers. The Damköhler number is simply the rate constant, k (1/hr), multiplied by a representative residence time, τ (hr), $Da = k\tau$. Bahr and Rubin (1987 [144539], p. 440, Equation 12) demonstrate that the mass balance equation describing solute transport can be differentiated into an equilibrium and a kinetic component. The smaller the kinetic component, the more accurate are the retardation factors based on the local equilibrium assumption.

For evaluation of colloid behavior, Damköhler numbers, Da_{att} and Da_{det}, can be computed for attachment and detachment of colloids, respectively, using k_{filt} and $k_{det.}$ The magnitude of the kinetic component is inversely proportional to $Da_{att}+Da_{det}$. Thus, the larger the sum of the two Damköhler numbers, the more appropriate the assumption of equilibrium. Bahr and Rubin (1987 [144539], p. 450) found that equilibrium was well approximated when the sum of the two Damköhler numbers is greater than 100 and reasonably well estimated when the sum is greater than 10. Valocchi (1985 [144579], p. 812-813, Figure 2) had a similar result, although he only used the reverse rate (detachment rate for colloids) to compute a Damköhler number. Bahr and Rubin (1987 [144539]) point out that the kinetic term can only be completely separated when the sum of the two Damköhler numbers is used.

Bahr and Rubin (1987 [144539]) caution that both Damköhler numbers, Da_{att}+Da_{det}, should be used to assess the kinetic term. In this analysis only Da_{att} is used, which should, therefore, be conservative. Another conservative aspect of this analysis is that there is no probability of a detachment rate constant of zero. In reality, it is very likely that some colloids will irreversibly attach.

To calculate Damköhler numbers for the fractured volcanics, the rate constants in Figure 2 are transformed to a Damköhler number distribution by multiplying the rate constants on the *x*-axis by an assumed travel time. We determine the fraction that has a Damköhler number greater than 100, which according to Valocchi (1985, [144579], p. 813, Figure 2) is a good approximation of equilibrium conditions. For a 100-year travel time, 96% of the colloids will have a Damköhler number greater than 100. For a 1000-year travel time, it will be over 98%; and for a 10-year travel time, it will 94%. An analysis of the alluvium rate constants results in very similar results with an even greater percentage with Damköhler numbers greater than 100. Thus, the vast majority of colloids that are not part of the unretarded fraction will transport in accordance with the local equilibrium assumption.

6.8 THE USE OF POLYSTYRENE MICROSPHERES AS TRACER SURROGATES FOR INORGANIC GROUNDWATER COLLOIDS

Many of the laboratory and field experiments used to develop the R_{col} distributions in this analysis use carboxylate-modified latex (CML) polystyrene microspheres to study colloid transport. This section describes the effectiveness of CML microspheres as analogs to inorganic groundwater colloids. CML microspheres were used as colloid tracers in the multiple-tracer tests in both the Bullfrog Tuff and the Prow Pass Tuff at the C-wells complex (BSC 2003 [162415], Section 6). CML microspheres were also used in one of the three single-well tracer tests in the saturated alluvium at NC-EWDP-19D1 (BSC 2003 [161620], Section 6.5), and they will be used in at least one cross-hole tracer test at the Alluvial Testing Complex (ATC). CML microspheres were selected as colloid tracers in these field tests because they are very monodisperse (i.e., they have a very narrow range of diameters) and they can be obtained with various fluorescent dyes incorporated into their polymer matrix, which allows them both to be detected at very low concentrations and to be discriminated from natural, nonfluorescing colloids using methods such as epifluorescent microscopy and flow cytometry. Flow cytometry has been used as the microsphere detection and quantification method for all field tracer tests in which microspheres have been used as tracers. This technique allows quantification at microsphere concentrations as low as 100 mL^{-1} in the presence of natural background colloid concentrations that are 2 to 4 orders of magnitude higher. These levels of detection and discrimination are currently not attainable using any other type of colloid tracer except perhaps viruses/bacteriophages (Bales et al. 1989 [104333], pp. 2063 to 2064).

CML microspheres were chosen over other types of polystyrene latex microspheres as field colloid tracers for two reasons: (1) they have surface carboxyl groups that give them a negative surface charge at pH greater than about 5 and (2) they have relatively hydrophilic surfaces compared to other types of polystyrene microspheres (Wan and Wilson 1994 [114430], p. 858, Table 1). These properties are consistent with those of natural inorganic groundwater colloids. The hydrophilic surfaces of CML microspheres are the result of their matrix being comprised of a copolymer of styrene and acrylic acid rather than pure styrene. This copolymer gives the CML

microspheres a higher surface density of carboxyl groups and also a significantly higher degree of surface hydrophilicity than other types of polystyrene microspheres, including "carboxylated" spheres that consist of a pure polystyrene matrix. In addition to providing better consistency with surface characteristics of inorganic colloids, these properties result in greater resistance to flocculation and less attachment to negatively charged, hydrophilic rock surfaces. Fluorescent dyes are generally incorporated into the microspheres by swelling the spheres in an organic solvent containing the dye and then washing the spheres in an aqueous solution to expel the solvent and shrink them back to their original size. Dye molecules tend to remain behind in the spheres because of their affinity for the organic matrix. As discussed above, the dyes in the matrix provide the means for discrimination of tracer colloids from natural colloids and for quantification of tracer colloid concentrations at very low levels.

The CML microspheres used in Yucca Mountain field tracer tests have all been purchased from Interfacial Dynamics Corp. (IDC) because IDC uses a surfactant-free synthesis process that does not require microspheres to be cleaned (by dialysis or centrifugation) to remove trace levels of surfactant before they are used in tests. Small levels of surfactants can greatly affect microsphere surface characteristics, resulting in inconsistency and irreproducibility of their transport behavior.

CML microspheres have properties that make them a suitable choice among synthetic polystyrene microspheres as reasonable surrogates for inorganic colloids. Table 10 provides a comparison of properties of CML microspheres and groundwater colloids. It is clear that although the two types of colloids differ in density, shape, and specific surface chemistry, they both have negative surface charges (at groundwater pHs) and hydrophilic surfaces.

Table 10. Comparison of Properties of CML Microspheres and Inorganic Groundwater Colloids

Property	CML Microspheres	Inorganic Groundwater Colloids
Size	Monodisperse but greater than 200-nm diameter to ensure good fluorescence detection	Polydisperse, ranging from < 50 nm to > 1 μm
Density	1.055 g/cm^3	2.0–2.6 g/cm^3
Shape	Spherical	Variable, including polygons, rods, and platelets
Surface Chemistry	Carboxyl groups with many polymer chains extending into solution	Variable, with silicate, iron oxide, aluminum oxide, manganese oxide, and other surface groups possible
Zeta potential	-30 mV or less in low ionic strength water at neutral pH	-30 mV or less in low ionic strength water at neutral pH
Hydrophobicity	Hydrophilic	Hydrophilic
pH at point of zero charge	~5.0	Variable, but generally less than 5 or 6

To address the suitability of using CML microspheres as surrogates for natural inorganic colloids, a limited number of laboratory experiments were conducted in which the transport behavior of CML microspheres was compared with that of silica microspheres in both saturated volcanic-tuff fractures and saturated alluvium-packed columns. All tests were conducted using the same CML microspheres (330-nm diameter microspheres from IDC dyed with a fluorescent yellow-green dye) and silica microspheres (100-nm diameter spheres from Nissan Chemical). Table 11 provides further information on the two colloid tracers. Silica microspheres were used for the comparison studies because previous testing had indicated that silica microspheres transport with much less attenuation through vertically oriented fractures than clay (montmorillonite) colloids (Kersting and Reimus 2003 [162421], pp. 222-223, 226-227, 230-231, Appendix C, Figures C-1, C-2, C-5, C-6, C-9, and C-10). Thus, if CML microspheres were shown to transport with less attenuation than silica microspheres, they would be expected to transport with far less attenuation than clay colloids.

The 330-nm CML microspheres were selected to be representative of microspheres with diameters ranging from about 250 to 500 nm, which represents a practical size range that can be used in field tests (detection-limited at the small end and cost-limited at the large end). Microspheres at the upper end of this size range will settle about twice as fast and diffuse about one-third slower than 330-nm diameter microspheres, and microspheres at the lower end of this range will settle about half as fast and diffuse about one-fourth faster than 330-nm diameter microspheres. Thus, the CML microspheres ranging in size from 250 to 500 nm (diameter) will both settle slower and diffuse slower than 100-nm silica microspheres. These characteristics (slower settling and diffusion) are both desirable from the standpoint of reducing the number of colloid collisions with aquifer surfaces. Thus, if electrostatic or double-layer interactions between colloids and aquifer surfaces are similar for both types of microspheres (as suggested by their similar zeta potentials, Table 11), the CML microspheres would be expected to transport with less attenuation relative to the silica microspheres.

6.8.1 Comparison of CML and Silica Microsphere Transport in Fractured Volcanic Rocks

Testing in fractured volcanic rock was conducted in two different fractured cores from Pahute Mesa at the Nevada Test Site, with the majority of the testing being done in a fractured lava. (At the time of the testing, fractured cores from the SZ near Yucca Mountain were not readily available.) Testing in the lava core was conducted at several different flow rates/residence times.

Details of the test procedures and the test results associated with the fractured volcanic core experiments are contained in Anghel (2001 [158639], Chapters 2 and 4), so they are only summarized here. Tables 12 through 14 provide information on the fractured cores, and Table 15 gives the major ion chemistry of the U-20WW water used in the fractured core experiments. Besides their differences in surface characteristics, the silica microspheres should have had greater diffusivity than the CML microspheres by a factor of about 3.3 because of their smaller size, and they also should have settled about 2.75 times faster than the CML microspheres because of their greater density. The two cores differed appreciably in their matrix porosities, with one having a relatively high porosity (0.369) and the other having a very low one (0.014). One experiment was conducted in the higher porosity core (ER-20-6 #1, 2406 ft below surface). Four experiments were conducted in the lower porosity core (PM-2, 7032 ft below surface). Test

details for each experiment are provided in Table 16. In addition to the colloid tracers, each experiment also included iodide ion as a conservative (nonsorbing) solute tracer. The responses of the colloid tracers could, thus, be compared to that of a conservative solute to allow better quantification of any colloid retardation or early arrival. All tracers were injected simultaneously so that they would have exactly the same injection input function. The iodide was analyzed by ion-selective electrode, the silica microspheres by high-sensitivity liquid in-situ particle spectrometery (HSLIS-S50, Particle Measuring Systems, Inc.), and the fluorescent microspheres by fluorometry (SPEX Fluorolog-2).

Table 11. Properties of CML and Silica Microspheres Used in Experiments

Property	CML Microspheres	Silica Microspheres
Particle Diameter (nm)	330 ± 11	100
% Solids (g/100g) (1)	2 ± 0.1	40.7
Stock Conc. (number/mL) (1)	1×10^{12}	3.8×10^{14}
Density (g/cm^3)	1.055	2.65
Dye Excitation/Emission Wavelengths (nm)	505/515	No Dye
Diffusion Coefficient (cm^2/s) (2)	1.34×10^{-8}	4.43×10^{-8}
Specific Surface Area (cm^2/g)	1.7×10^{5}	2.3×10^{5}
Surface Charge (meq/g) (4)	0.08	NM(3)
Zeta Potential in U-20WW Water (mV) (5)	-42.7 ± 9.1	-41.2 ± 4.1
Zeta Potential in NC-EWDP-19D1 Water (mV)	NM	-45.15 ± 2.9

Source: All information comes from manufacturers' certificates of analyses or was calculated as described below except for zeta potentials. Zeta potentials are reported by Anghel (2001[158639], Chapter 2).

NOTE: (1) Manufacturer's stock solution in deionized water; solutions used in experiments were diluted in groundwater to several orders of magnitude below these concentrations.

(2) Calculated using the Stokes-Einstein equation, $D = kT/(6\pi\mu R)$, where k = Boltzmann's constant (1.38×10^{-16} ergs/K), T = temperature (°K), μ = fluid viscosity (g/cm-s), and R = colloid radius (cm). Calculations assume water at 25°C (298°K).

(3) NM = not measured.

(4) Value reported by the manufacturer (Interfacial Dynamics Corp.).

(5) The zeta potential is the potential measured at the "surface of shear" near the colloid surface in solution (Hiemenz 1986 [117358], p. 745). The surface of shear occurs where ions transition from being immobile to being mobile relative to the colloid surface when the colloid moves relative to the surrounding solution. The zeta potential is generally considered to be the best experimental measure of the strength of electrostatic interactions between colloids or between colloids and surfaces in solution.

Table 12. Properties of the Fractured Cores Used in the Colloid Transport Experiments: Physical Characteristics

Fracture (Depth below land surface)	Fracture Length (cm)	Fracture Width (cm)	Matrix Porosity
PM-2 (7032 ft)	14	9	0.014
ER-20-6#1 (2406 ft)	23.8	12.7	0.369

Source: Notebook SN-LANL-SCI-280-V1 (Reimus 2003 [163760], Attachment E).

Table 13. Properties of the Fractured Cores Used in the Colloid Transport Experiments: X-ray Diffraction Results (wt %)

Fracture	Smec-tite	Zeo-lite	Opal	Quartz	K-Spar	Plagio-clase	Hema-tite	Bio-tite	Calcite	Chlorite	Epidote/ Clinozoisite	Total
PM-2 7032 ft	—	—	—	22.1	18.8	38.3	—	2.0	1.2	6.7	9.6	98.7
ER-20-6#1 2406 ft	1.7	83.4	27.3	0.9	4.8	3.3	—	1.5	—	—	—	102.7

Source: Notebook SN-LANL-SCI-280-V1 (Reimus 2003 [163760], Attachment E).

NOTE: — = not detected

Table 14. Properties of the Fractured Cores Used in the Colloid Transport Experiments: Lithologic Descriptions

Fracture	Description
PM-2 7032 ft	Devitrified intermediate composition lava from the andesite of Mt. Helen of the Volcanics of Quartz Mountain.
ER-20-6#1 2406 ft	Highly zeolitic, poor to moderately-welded vitric, lithic tuff from the Calico Hills Formation.

Source: Anghel (2001 [158639], Chapter 2)

Table 15. Chemical Composition of U-20WW Groundwater

Constituent	Concentration (mg/L)
Ca^{2+}	7.18 ± 0.05
K^{+}	1.3 ± 0.1
Na^{+}	60 ± 0.3
SiO_2	46.9
Cl^{-}	11.6 ± 0
F^{-}	2.6 ± 0
HCO_3^{-}	110
SO_4^{2-}	32
PH	7.96
Specific Conductance (μS/cm)	296
TDS (mg/L)	273.8
Ionic Strength	~0.0035

Source: Notebook SN-LANL-SCI-280-V1 (Reiums 2003 [163760], Attachment E).

Table 16. Summary of Experimental Conditions in the Fractured Core Tests

ER-20-6#1, 2406 ft

Flow Rate (mL/hr)	4.96
Fracture Orientation	Vertical
Injection Duration (hr)	10.0
Injection Concentration [(1)]	127 mg/L (I^-) 4.22 x 10^7 mL^{-1} (0.33-µm CML microspheres) 5.2 x 10^{10} mL^{-1} (0.1-µm silica microspheres)
Tracer Recoveries (Fractional)	0.85 (I^-) 0.63 (CML microspheres) 0.72 (silica microspheres)

PM-2, 7032 ft

Experiment Number	**1**	**2**
Flow Rate (mL/hr)	10.02	2.5
Fracture Orientation	Vertical	Vertical
Injection Duration (hr)	3.3	13.2
Injection Concentration[(1)]	127 mg/L (I^-) 1.6 x 10^7 mL^{-1} (0.33-µm CML microspheres) 6.9 x 10^{10} mL^{-1} (0.1-µm silica microspheres)	127 mg/L (I^-) 1.9 x 10^7 mL^{-1} (0.33-µm CML microspheres) 7.9 x 10^{10} mL^{-1} (0.1-µm silica microspheres)
Tracer Recoveries (Fractional)	1.09 (I^-) 1.09 (CML microspheres) 1.06 (silica microspheres)	1.06 (I^-) 0.89 (CML microspheres) 0.88 (silica microspheres)
Experiment Number	**3**	**4**
Flow Rate (mL/hr)	0.58	0.57
Fracture Orientation	Vertical	Horizontal
Injection Duration (hr)	56	56
Injection Concentration[(1)]	127 mg/L (I^-) 1.9 x 10^7 mL^{-1} (0.33-µm CML microspheres) 7.4 x 10^{10} mL^{-1} (0.1-µm silica microspheres)	127 mg/L (I^-) 1.7 x 10^7 mL^{-1} (0.33-µm CML microspheres) 7.5 x 10^{10} mL^{-1} (0.1-µm silica microspheres)
Tracer Recoveries (Fractional)	0.96 (I^-) 0.77 (CML microspheres) 0.60 (Silica microspheres)	0.93 (I^-) 0.77 (CML microspheres) 0.24 (Silica microspheres)

Source: Notebook SN-LANL-SCI-280-V1 (Reimus 2003 [163760], Attachment E).

NOTE: [(1)] Calculated concentrations for microspheres are as much as 20–30% of error. However, the normalized concentrations should be accurate to within 5%.

Figures 8 through 12 show the responses of each of the tracers in each of the five fractured core experiments. It is clear that at higher flow rates and shorter residence times, the CML microspheres and the silica microspheres transported almost identically in vertically oriented fractures, with minimal attenuation of either microsphere. However, both microspheres became more attenuated at the lower flow rates (~0.6 mL/hr), with the CML microspheres being consistently less attenuated than the silica microspheres. It is also apparent from Figures 11 and 12 that the silica microspheres were more attenuated in the horizontal orientation of the low-porosity fracture than in the vertical orientation at the same flow rate. The reason for different behavior between the horizontal and vertical cores is that the vertical orientation of the core leads to less resistance to downward water flow through the column. In this case, a horizontal orientation means that the fractured core was oriented such that the fracture surfaces were parallel to the lab bench top, whereas a vertical orientation means that the core was oriented so that the fracture surfaces were perpendicular to the lab bench top.

Quantitative interpretation of the tests in the lower-porosity fracture were carried out by Anghel (2001 [158639], Chapter 4) using the RELAP (STN: 10551-2.0-00) computer code. The interpretive method is described in detail in Section 6.4.1. The resulting fitted parameter values are listed in Table 17. The single test in the higher-porosity fracture was only qualitatively interpreted because a single test at a constant flow rate does not allow unambiguous estimation of solute or colloid transport parameters. However, it is clear from Figure 8 that there was no significant difference in the transport of the two colloid tracers in this fracture. Also, the iodide appeared to experience a significant amount of matrix diffusion in this fracture based on its attenuated peak normalized concentration relative to the colloids and its extended tailing behavior. Microsphere recoveries in this fracture suggested a colloid-filtration rate constant of ~0.2 hr^{-1}.

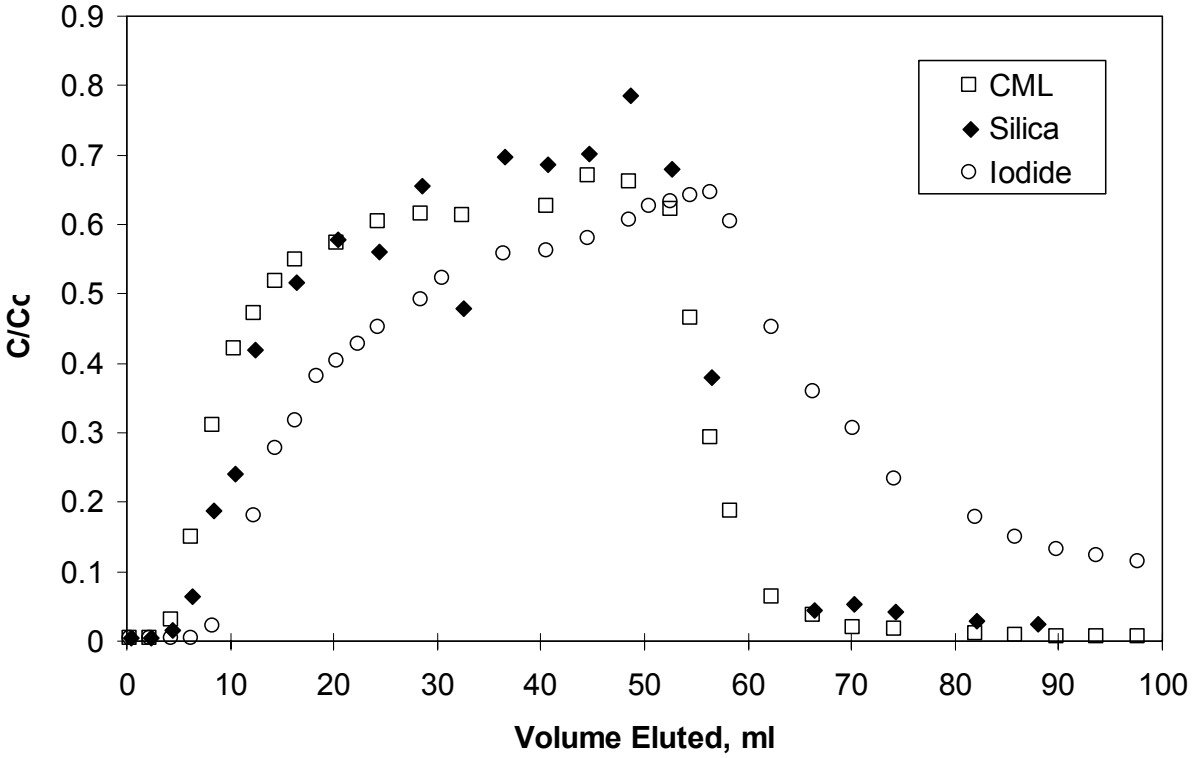

DTN: LA0301PR831352.001

NOTES: The flow rate was ~5 mL/hr, and the tracer injection pulse was ~50 mL.

Normalized concentrations of silica less than about 0.03 in this figure are subject to error because background colloid concentrations begin to approach silica concentrations at these levels.

Figure 8. Normalized Concentrations of 330-nm Diameter CML Microspheres, 100-nm Diameter Silica mirocspheres, and Iodide in Vertically Oriented Fractured Core from ER-20-6#1 at 2406 ft

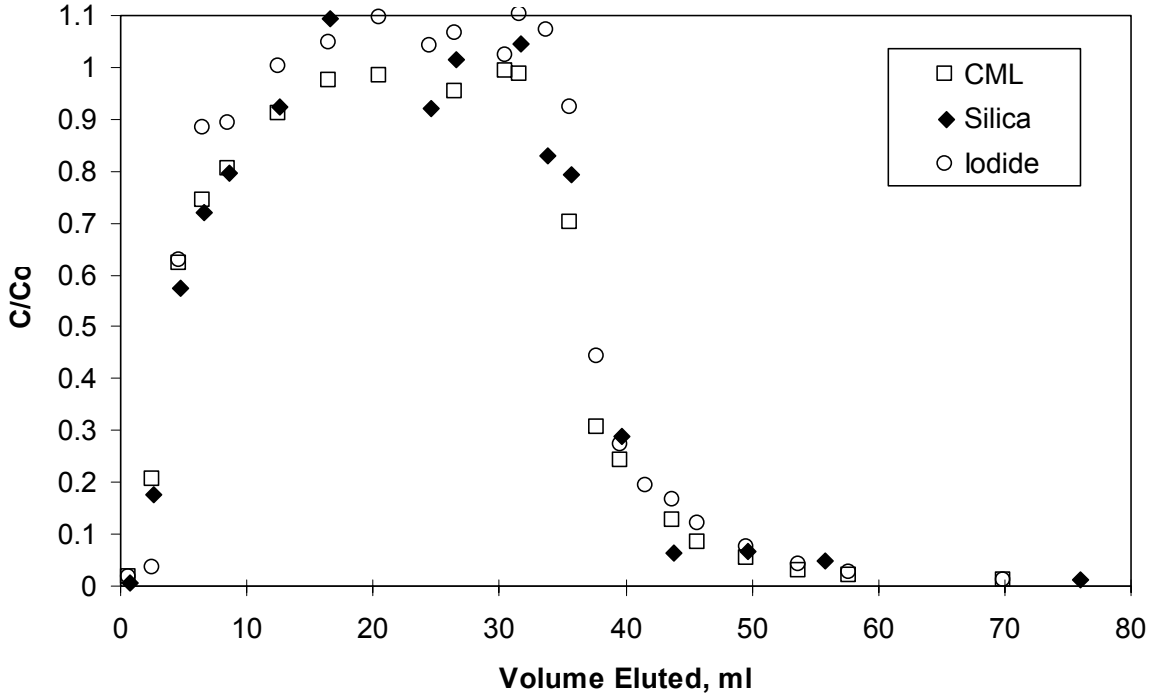

DTN: LA0301PR831352.001

NOTE: The flow rate was ~10 mL/hr, with a mean tracer residence time of ~0.6 hr. The tracer injection pulse was ~33 mL.
Normalized concentrations of silica less than about 0.03 in this figure are subject to error because background colloid concentrations begin to approach silica concentrations at these levels.

Figure 9. Normalized Concentrations of 330-nm Diameter CML Microspheres, 100-nm Diameter Silica Microspheres, and Iodide in Vertically Oriented Fractured Core from PM-2 at 7032 ft at 10mL/hr

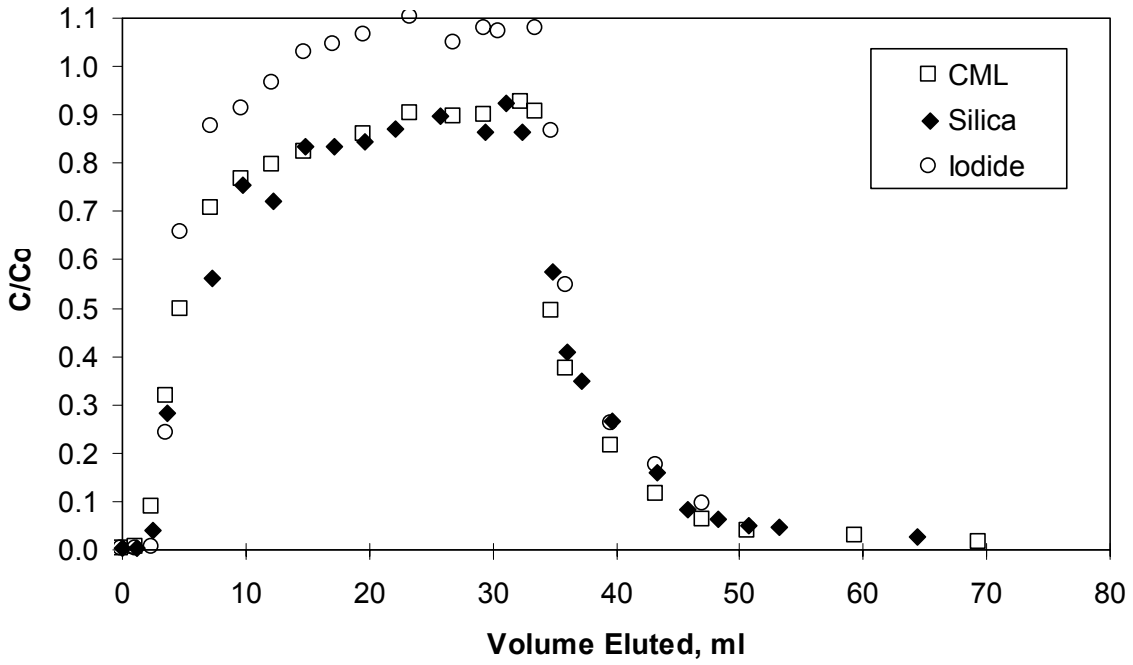

DTN: LA0301PR831352.001

NOTE: The flow rate was ~2.5 mL/hr, with a mean tracer residence time of ~2.4 hr. The tracer injection pulse was ~33 mL.
Normalized concentrations of silica less than about 0.03 in this figure are subject to error because background colloid concentrations begin to approach silica concentrations at these levels.

Figure 10. Normalized Concentrations of 330-nm Diameter CML Microspheres, 100-nm Diameter Silica Microspheres, and Iodide in Vertically Oriented Fractured Core from PM-2 at 7032 ft at 2.5 mL/hr

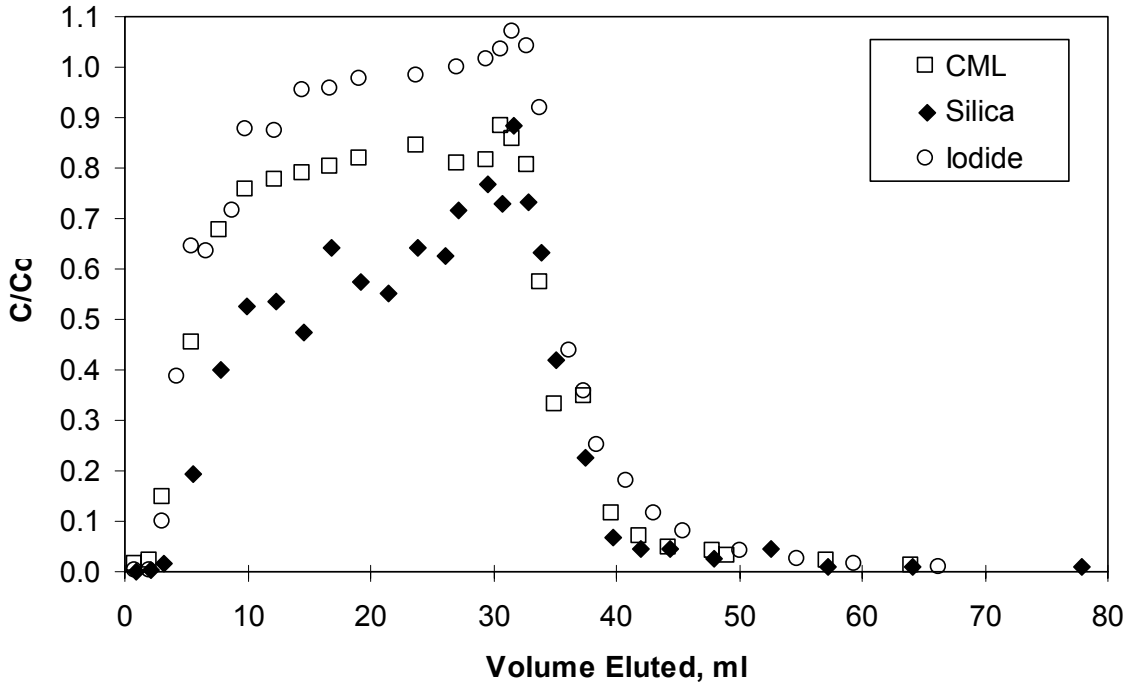

DTN: LA0301PR831352.001

NOTE: The flow rate was ~0.6 mL/hr, with a mean tracer residence time of ~10.4 hr. The tracer injection pulse was ~33 mL, and the orientation of the core was vertical.
Normalized concentrations of silica less than about 0.03 in this figure are subject to error because background colloid concentrations begin to approach silica concentrations at these levels.

Figure 11. Normalized Concentrations of 330-nm Diameter CML Microspheres, 100-nm Diameter Silica Microspheres, and Iodide in Vertically Oriented Fractured Core from PM-2 at 7032 ft at ~0.6 mL/hr

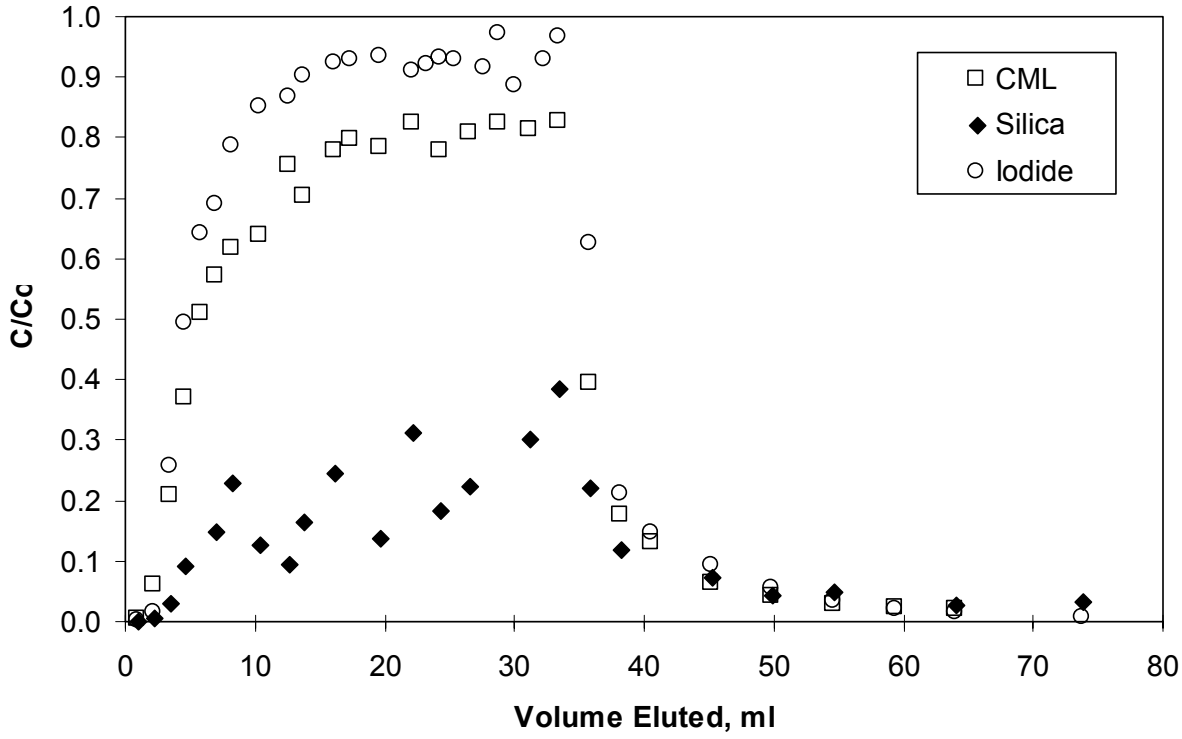

DTN: LA0301PR831352.001

NOTE: The flow rate was ~0.6 mL/hr, with a mean tracer residence time of ~10.3 hr. The tracer injection pulse was ~33 mL, and the orientation of the core was horizontal.
Normalized concentrations of silica less than about 0.03 in this figure are subject to error because background colloid concentrations begin to approach silica concentrations at these levels.

Figure 12. Normalized Concentrations of 330-nm Diameter CML Microspheres, 100-nm Diameter Silica Microspheres, and Iodide in Horizontally Oriented Fractured Core from PM-2 at 7032 ft at ~0.6 mL/hr

Table 17. Model Parameters from RELAP Fits of Tracer Breakthrough Curves in Experiments in Fractured Core from Borehole PM-2

Model Parameter	Flow Rate (mL/hr)			
	10.0	**2.5**	**0.58 (V)**	**0.57 (H)**
Mean Fluid Residence Time (hr)	0.60	2.43	10.43	10.27
Fracture Half Aperture (cm)	0.024	0.024	0.024	0.024
Iodide Peclet Number	14.0	9.5	9.5	9.5
Iodide Dispersivity (cm)	1.0	1.5	1.5	1.5
Colloid Peclet Number	2.88	2.88	2.88	2.88
Colloid Dispersivity (cm)	4.86	4.86	4.86	4.86
Iodide Matrix Diffusion Coefficient ($cm^2/s \times 10^7$)	5.9	14.4	14.4	14.4
CML Microsphere Filtration Rate Constant (hr^{-1})	0.080	0.065	0.021	0.026
Silica Microsphere Filtration Rate Constant (hr^{-1})	0.090	0.085	0.051	0.201

DTN: LA0303PR831352.003, excel files used: PM1_PM2.xls, PM-2 Iodide.xls, PM-2 Microspheres.xls.

NOTES: (1) V = vertical orientation; H = horizontal orientation.

(2) Fracture half-aperture calculated from $b = \frac{Q\tau}{2LW}$, where Q = volumetric flow rate, mL/hr, τ = mean residence time, hr, L = fracture length, cm, and W = fracture width, cm. Mean fluid residence times were estimated from simultaneous RELAP fits to the iodide breakthrough curves at different flow rates.

Before drawing conclusions from the results of the fracture transport experiments, it is useful to define two characteristic length quantities:

$$L_D = \sqrt{2D\tau} \quad \text{(Eq. 5)}$$

$$L_S = V_S\tau = \left(\frac{1}{18\mu}\right)(\rho_P - \rho_f)gd_p^2\tau \quad \text{(Eq. 6)}$$

where

L_D = characteristic diffusion length during time τ, cm

L_S = characteristic gravitational settling length during time τ, cm

D = colloid diffusion coefficient (calculated using Stokes-Einstein equation – see footnote 2 of Table 11), cm^2/s

τ = fluid residence time in fracture, s

V_S = settling velocity, cm/s

μ = fluid viscosity, g/cm-sec

ρ_p = particle density, g/cm^3

ρ_f = fluid density, g/cm^3

g = gravitational acceleration, cm/s^2

d_p = colloid diameter, cm.

The characteristic lengths L_D and L_S differed for the two microsphere tracers in each of the fracture transport tests in the lower-porosity fracture (Table 18).

Table 18. Characteristic Diffusion and Settling Lengths (L_D and L_S) for the CML and Silica Microspheres in the Four Experiments in the Fractured Core from Borehole PM-2

Microsphere Characteristic Lengths	Flow Rate (mL/hr)			
	10.0	2.5	0.58 (V)	0.57 (H)
CML Diffusion Length, L_D (cm)	0.008	0.015	0.032	0.032
Silica Diffusion Length, L_D (cm)	0.014	0.028	0.058	0.057
CML Settling Length, L_S (cm)	0.0007	0.0028	0.012	0.012
Silica Settling Length, L_S (cm)	0.0019	0.0078	0.034	0.033

Source: Anghel (2001 [158639], Tables 5.2 and 5.5)

NOTE: The average fracture aperture ($2b$) was estimated to be 0.048 cm.
V = vertical orientation; H = horizontal orientation.

With these quantities defined, the following conclusions from the experiments can now be stated.

- When the fractures were in the vertical orientation, similar colloid responses were obtained at the same flow rate/residence time provided that $L_D/2b < 1$ for both microspheres, where $2b$ = average fracture aperture (b = half aperture). At flow rates where $L_D/2b > 1$ for the silica and $L_D/2b < 1$ for the CML microspheres, the latter transported with much less attenuation than the former.

- The fracture orientation influenced only the silica colloid transport, which is consistent with the greater silica settling velocity and the fact that $L_S/2b \approx 1$ for the silica microspheres and $L_S/2b < 1$ for the CML microspheres. A significant fraction of the silica microspheres was apparently able to settle to the lower surface of the horizontally oriented fracture during their residence time in the flow system, whereas most of the CML microspheres did not settle during this time.

- The "sticking efficiencies" (fractions of colloid-wall collisions that resulted in attachment) of the two colloids appeared to be quite similar. This conclusion is based on comparing the experimental results to colloid deposition theory in a parallel-plate channel in the absence of gravitational effects, which predicts that the filtration rate constant, k_f, should be proportional to $\left(\tau d_p^2\right)^{-1/3}$ if all colloid-wall collisions result in irreversible attachment; i.e., a "perfect-sink" boundary condition (Van de Ven 1989 [158637], pp. 452-453, Equation 6.20 and Table 6.2; definition of Pe for parallel-plate channel on p. 446, Table 6.1, and diffusion coefficient dependence on d_p, p. 77, Equation 2.112).

This proportionality of k_f to $\left(\tau d_p^2\right)^{-1/3}$ in the absence of gravity effects is derived from Van de Ven (1989) as follows:

Van de Ven (p. 452, Equation 6.20) shows that the deposition flux, J, in a parallel-plate channel is given by $J = \frac{Sh\, D\, n_\infty}{r} = k_f n_\infty$, where Sh = Sherwood number (dimensionless), D = colloid diffusion coefficient, cm^2/s, n_∞ = colloid concentration in bulk solution, mL^{-1}, and r = colloid radius. The Sherwood number for a parallel-plate channel is equal to $\frac{0.678\, Pe^{1/3}}{\widetilde{x}^{1/3}}$ (Van de Ven, 1989, Table 6.2, p. 453), where $Pe = \frac{3 v_m r^3}{2b^2 D}$ (Van de Ven, 1989, Table 6.1, p. 446), $\widetilde{x} = x/L$, v_m = mean flow velocity in channel, cm/s, and b = channel half-aperture, cm. Substituting the expression for Pe into the expression for Sh, one obtains $Sh = \frac{C v_m^{1/3} r}{b^{2/3} D^{1/3} \widetilde{x}^{1/3}}$, where C is a proportionality constant. Recognizing that any given distance x down the parallel-plate channel will be equal to $v_m \tau$, where τ is the time required to travel the distance x, then $Sh = \frac{C' r}{b^{2/3} D^{1/3} \tau^{1/3}}$ and $J = k_f n_\infty = C'' \frac{D^{2/3}}{b^{2/3} \tau^{1/3}} n_\infty$. Now, substituting the Stokes-Einstein equation (see footnote 2 of Table 11) for D in this expression yields $J = k_f n_\infty = C''' \left(\frac{1}{\tau^{1/3} r^{2/3}}\right) n_\infty$, from which it is readily apparent that $k_f \propto \left(\tau\, d_p^2\right)^{-1/3}$, where d_p is the colloid diameter.

The quantity d_p^2 for the CML microspheres was 10.9 times greater than that for the silica microspheres, so if the two microspheres had the same "sticking efficiency", they would be predicted to have the same k_f values when the residence time τ of the CML microspheres is 10.9 times less than that for the silica. In fact, when the residence time was approximately 9 times less for the CML microspheres, the filtration rates constants were 0.06 and 0.051 hr^{-1} for the CML and silica microspheres, respectively. These rate constants are in relatively good agreement with each other (within experimental error), which suggests that the "sticking efficiencies" of the two microspheres were very similar. Note that the CML rate constant of 0.06 hr^{-1} was obtained in an experiment conducted at a flow rate of approximately 5 mL/hr in which only CML microspheres and iodide were used as tracers. This experiment is not presented or discussed elsewhere in this analysis report because it did not involve a direct comparison of CML and silica microspheres (all other experiments involved simultaneous injection of both microsphere tracers). For details of the experiment, see Anghel (2001 [158639], Sections 2.10 and 4.6).

- The above three conclusions suggest that CML microspheres on the order of 250 to 500 nm in diameter should transport either similarly to or with less attenuation than natural inorganic groundwater colloids in saturated fractured systems.

6.8.2 Comparison of CML Microsphere and Inorganic Colloid Transport in Saturated Alluvium

Two separate sets of experiments were conducted in which the transport of CML microspheres were compared to that of natural inorganic colloids in saturated alluvium. The natural colloids were collected from water discharged from NC-EWDP-19D1 during the last few weeks of a single-well tracer test, after tracer concentrations had decayed to the point where they contributed insignificantly to the ionic strength of the ground water. A portion of the discharged water was first directed through a 1-micron cartridge pre-filter to remove all larger entrained solids. The pre-filtered water was then passed through a high-surface-area membrane filter with a pore size rating of 5-10 nm to trap colloids in the ground water. The membrane filter was allowed to collect colloids until flow through it became significantly restricted. At this point, the filter was backflushed (flow reversed using pre-filtered groundwater) to dislodge the colloids from the filter. The backflushing produced a highly concentrated colloid solution that was collected in a container. The filtration and backflushing process was then repeated until over 100 liters of concentrated colloid solution had been collected. In the first set of experiments, 330-nm diameter CML microspheres and 100-nm diameter silica microspheres were simultaneously injected into columns packed with alluvium from the uppermost screened interval of NC-EWDP-19D1. Water from the same interval was used in these experiments. The CML and silica microspheres were the same microspheres that were used in the fracture transport experiments discussed in Section 6.8.1 (see Table 11). In the second set of experiments, 190-nm and 500-nm diameter CML microspheres were injected simultaneously with natural colloids collected from NC-EWDP-19D1. The alluvium and water in these experiments were taken from the lowest screened interval completed in the alluvium at the ATC (the water came from NC-EWDP-19D1, and the alluvium came from NC-EWDP-19IM1A). In this set of experiments, Pu(V) was sorbed onto the natural colloids prior to the colloids being injected into the columns. Thus, these experiments also provided a test of colloid-facilitated Pu transport in saturated alluvium, although the Pu transport results are not discussed in this analysis report. The results from the first set of experiments (involving CML and silica microspheres) are discussed in Section 6.8.2.1, and the results from the second set of experiments involving the Pu-tagged natural colloids and CML microspheres are discussed in Section 6.8.2.2.

6.8.2.1 CML and Silica Microsphere Transport in Saturated Alluvium

Column experiments were conducted in two separate 30-cm long by 2.5-cm diameter glass columns equipped with polytetrafluoroethylene end fittings, including a 20-μm end frit and polytetrafluoroethylene tubing. The alluvium used in the experiments was obtained from NC-EWDP-19D1 at the depth intervals of 405 to 410 and 420 to 425 ft below ground surface, approximately 50 to 75 ft below the water table. Cuttings samples were wet sieved (using NC-EWDP-19D1 well water) in the laboratory, and the size range between 75 and 2000 μm was retained for testing. Material from the two intervals was combined in a 50:50 mass ratio for the column experiments because there was not enough material from the individual intervals to pack the columns. The packed porosities of the two columns were 0.404 and 0.418. The water used in testing was taken from the uppermost screened interval of well NC-EWDP-19D1, which was the same interval that the alluvium material came from.

The column experiments involved the simultaneous introduction of a pulse (~60 mL) of groundwater containing the same 330-nm diameter CML microspheres and 100-nm diameter silica microspheres used in the fracture experiments along with sodium bromide, with bromide ion serving as a nonsorbing solute tracer. Bromide was analyzed by ion chromatography, the CML microspheres were analyzed by fluorometry, and the silica microspheres were analyzed by high-sensitivity liquid in-situ spectrometry. The first two experiments were conducted at flow rates of 2 and 6 mL/hr in Columns A and B, respectively. The normalized concentration responses of the colloids and bromide in these two experiments are shown in Figures 13 and 14. Not surprisingly, the normalized concentrations of both colloid tracers were greater in the column with the higher flow rate (Column B). However, in contrast to the fracture transport experiments, the CML microspheres were more attenuated than the silica microspheres in both columns. The greater attenuation of the CML microspheres relative to the silica microspheres could be the result of enhanced deposition of the larger microspheres by interception (collisions with alluvium grains as a result of flow streamlines bringing the microspheres into contact with the grain surfaces). Interception in a porous medium is predicted to be proportional to $(d_p/d)^2$ (Harvey and Garabedian 1991 [109256]), where d_p is the colloid diameter and d is the grain size of the porous medium. The microsphere recoveries in the experiments were not calculated, but as a first approximation, they are about equal to the peak normalized concentrations of microspheres. Clearly, the recoveries are much lower than in the fracture transport experiments of Section 6.8.1.

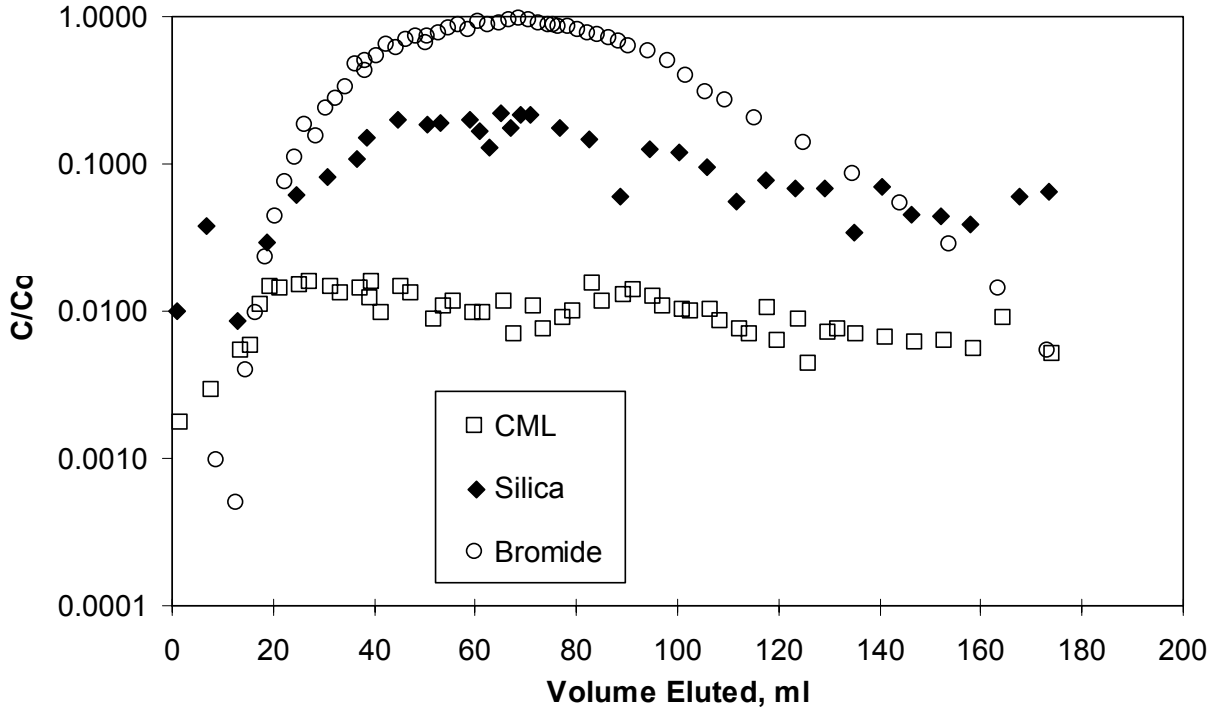

DTN: LA0206MH831361.001

NOTE: The flow rate was ~2 mL/hr.
Normalized concentrations of silica less than about 0.03 in this figure are subject to error because background colloid concentrations begin to approach silica concentrations at these levels.

Figure 13. Log Normalized Concentrations of 330-nm Diameter CML Microspheres, 100-nm Diameter Silica Microspheres, and Bromide in Alluvium-Packed Column A

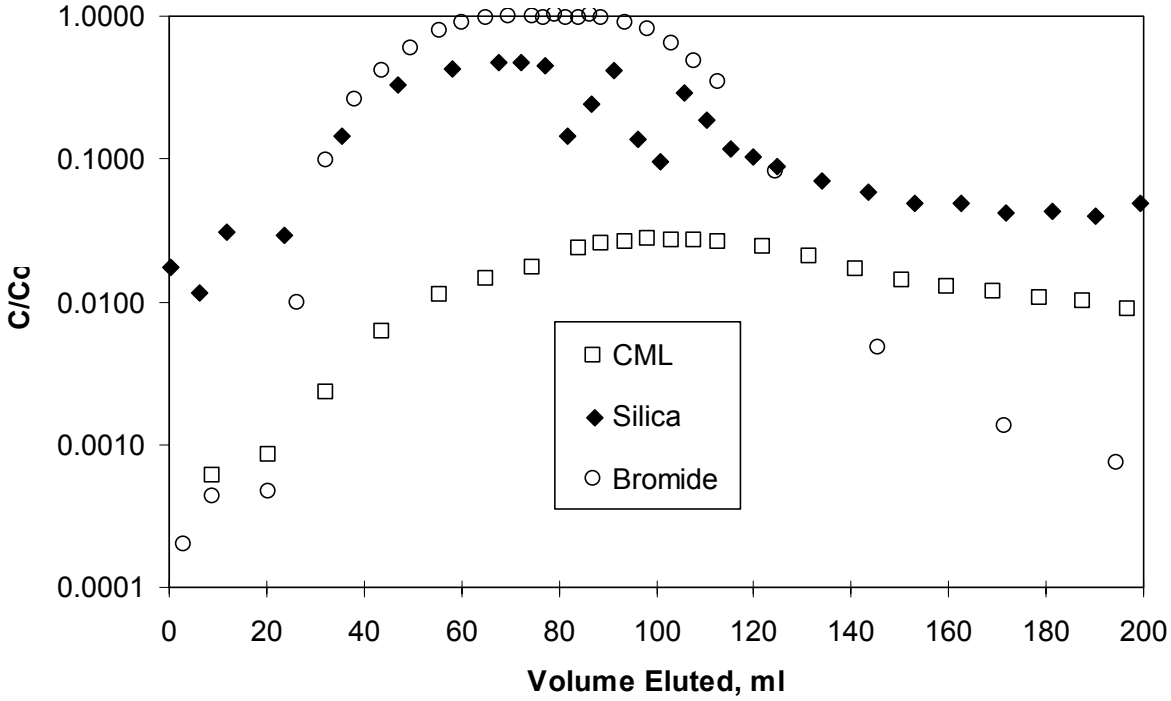

DTN: LA0206MH831361.002

NOTE: The flow rate was ~6 mL/hr.
Normalized concentrations of silica less than about 0.03 in this figure are subject to error because background colloid concentrations begin to approach silica concentrations at these levels.

Figure 14. Log Normalized Concentrations of 330-nm Diameter CML Microspheres, 100-nm Diameter Silica Microspheres, and Bromide in Alluvium-Packed Column B

For the fracture transport experiments (both horizontal and vertical orientations), colloid interception played an insignificant role in deposition because the average fracture aperture was on the order of 0.5 mm (i.e., very large compared to the colloid diameters) and the fracture walls were primarily parallel to flow. However, in a porous medium, flow can follow much more tortuous pathways around grains, and pore throats around small grains may be quite narrow. Although sieving of the material used to pack the columns was intended to exclude grain sizes smaller than 75 μm in diameter, it is likely that finer material was present in the columns or perhaps generated after the columns were allowed to flow. Also, because of the irregular shapes of the alluvium grains, most pore throats were probably quite a bit narrower than would be predicted assuming spherical grains. These factors may have resulted in a significant number of collisions of the CML microspheres due to interception with the alluvium grains in the columns. The silica microspheres, however, had a value of $(d_p/d)^2$ about a factor of 11 less than that of the CML microspheres, so interception would be expected to play a much less important role in their deposition.

A second set of CML and silica microsphere transport experiments was conducted in the two alluvium-packed columns. The second experiment in Column B was conducted at the same flow rate as the first experiment in this column (~6 mL/hr), whereas the second experiment in Column A was conducted at a flow rate of ~12 mL/hr, approximately 6 times greater than in the first experiment. The normalized concentration responses of the tracers in these two experiments are shown in Figures 15 and 16. When comparing the first and second experiments in Column B (Figures 14 and 16), it is apparent that both colloids were appreciably more attenuated in the second experiment, and the CML microspheres became even more attenuated relative to the silica microspheres. The peak concentration of the silica microspheres in this column decreased by about a factor of 3 in the second experiment, whereas the peak concentration of the CML microspheres decreased by nearly a factor of 10 compared to the first experiment. These decreases might be attributed to a decrease in the hydraulic conductivity of the columns, which often occurs over time due to microbial growth or redistribution of fines, both of which tend to decrease effective pore throat diameters in columns. The hydraulic conductivity of both columns was measured only after the second test, not prior to either test, so it was not possible to unequivocally attribute the decrease in colloid recoveries in Column B to a decrease in hydraulic conductivity.

Despite the fact that the flow rate in the second experiment in Column A was about six times greater than in the first experiment, the peak concentration of CML microspheres was only marginally higher than in the first test, and the peak concentration of silica microspheres was lower (compare Figures 13 and 15). Normally, one would expect greater peak concentrations of both microspheres at a higher flow rate in the same column. Also, unlike the other three alluvium column tests, the peak concentration of CML microspheres was higher than the silica peak concentration silica in the second test in Column A. The microsphere responses in the second test were probably influenced by the presence of air pockets that appeared in both the top and bottom ends of the column some time after the first experiment had been completed. These air pockets were presumably the result of slow leaks that occurred in the top and bottom end fittings of the columns.

The lower-than-expected peak concentrations of both microspheres in the second test in Column A and the fact that the silica microspheres were more attenuated than the CML microspheres in this test are attributed to the attachment of both microspheres to the air-water interfaces present at either end of the column. Colloids that come into contact with air-water interfaces become essentially irreversibly attached to the interface as a result of strong capillary forces (Abdel-Fattah and El-Genk 1998 [158692], pp. 248-250). The silica microspheres would be expected to collide more frequently with these interfaces than the CML microspheres because of their greater diffusivity, thus resulting in greater attenuation relative to the CML microspheres.

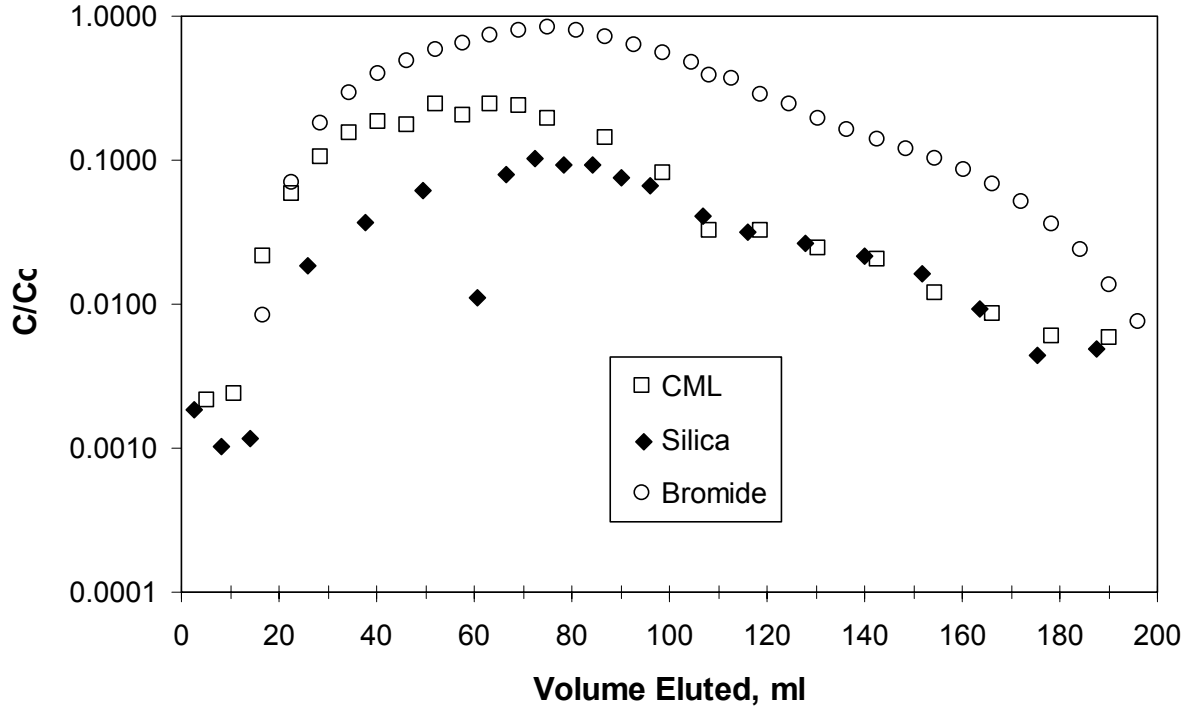

DTN: LA0206MH831361.003

NOTE: The flow rate was ~12 mL/hr.
Normalized concentrations of silica less than about 0.03 in this figure are subject to error because background colloid concentrations begin to approach silica concentrations at these levels.

Figure 15. Log Normalized Concentrations of 330-nm Diameter CML Microspheres, 100-nm Diameter Silica Microspheres, and Bromide in Second Experiment in Alluvium-Packed Column A

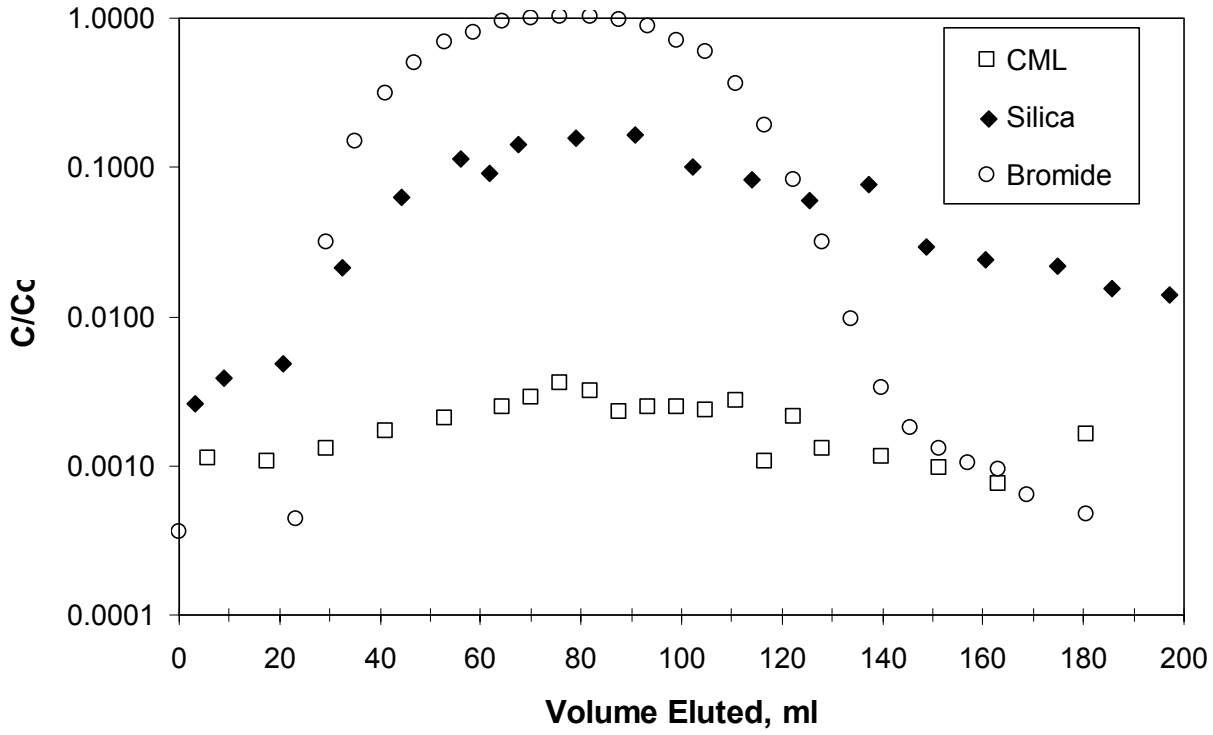

DTN: LA0206MH831361.004

NOTE: The flow rate was ~6 mL/hr.
Normalized concentrations of silica less than about 0.03 in this figure are subject to error because background colloid concentrations begin to approach silica concentrations at these levels.

Figure 16. Log Normalized Concentrations of 330-nm Diameter CML Microspheres, 100-nm Diameter Silica Microspheres, and Bromide in Second Experiment in Alluvium-Packed Column B

Table 19 provides estimates of filtration and detachment rate constants for the CML and silica microspheres in each of the alluvium column experiments. These estimates were obtained by fitting the experimental data using the approach described in Section 6.4.1. That is, the RELAP (STN: 10551-2.0-00) computer code was used to fit the bromide responses to estimate the mean residence times and Peclet numbers in the column tests, and then the colloid filtration rate constants and retardation factors were adjusted to fit the colloid responses. The retardation factors were constrained by fitting the tails of the colloid responses. Detachment rate constants were then obtained by rearrangement of Equation 4. It should be recognized that the detachment rate constants for silica are very crude estimates because the silica tails rapidly approached background colloid concentrations. Table 19 also provides the effective partition coefficients (K_d values) for the colloids in each experiment, given by the filtration rate constant divided by the detachment rate constant. These retardation factors would apply to large time scales if it is assumed that filtration is completely reversible.

Table 19. Estimates of Filtration Rate Constants and Detachment Rate Constants for CML Microspheres and Silica Colloids in Columns Packed with Alluvium

Colloid Transport Parameters	Column / Flow Rate			
	A / 2 mL/hr	B / 6 mL/hr	A / 12 mL/hr	B / 6 mL/hr
CML filtration rate constant (hr^{-1})	0.68	0.6	0.38	0.91
CML detachment rate constant (hr^{-1})	0.004	0.019	0.0027	0.0065
CML Retardation Factor	170	33	140	140
Silica filtration rate constant (hr^{-1})	0.22	0.13	0.73	0.28
Silica detachment rate constant (hr^{-1})	0.0022*	0.0081	0.0037	0.0156
Silica Retardation Factor	100	17	200	19

DTN: LA0303PR831361.001

NOTE: *This value cannot be practically distinguished from zero.
NOTE: The filtration rate and retardation factor are fit using RELAP and the detachment rate constant is calculated using equation 3.

It is apparent from Figures 13 through 16 and Table 19 that the relative transport behavior of the CML microspheres and the silica microspheres was appreciably different in the alluvium columns from that in the fractured cores. These differences are attributed to smaller pore throat sizes in the alluvium columns and, hence, greater interception of the CML microspheres in these columns. The results indicate that CML microspheres with diameters greater than ~300 nm will not necessarily behave as conservative surrogates for natural groundwater colloids in the saturated alluvium south of Yucca Mountain.

6.8.2.2 CML Microsphere and Natural Colloid Transport in Saturated Alluvium

A second set of colloid transport experiments was conducted to further investigate and compare the transport of CML microspheres and inorganic colloids in saturated alluvium. This set of experiments had several objectives.

1. There was concern that air bubbles in the columns in the first set of experiments (Section 6.8.2.1) may have influenced the results. Thus, a second set of experiments in which more emphasis was placed on eliminating air bubbles was desired.

2. Natural colloids from NC-EWDP-19D1, which were collected to be used in a cross-hole field tracer test, became available after the first set of tests. These colloids were more representative of natural colloids in the alluvium than the synthetic silica colloids used in the first set of experiments, so it was desirable to conduct a second set of experiments using these colloids.

3. It was desirable to use lower concentrations of CML microspheres than in the first set of tests to minimize any interactions between the microspheres and inorganic colloids. This could be accomplished by using flow cytometry to determine microsphere concentrations instead of fluorometry. Flow cytometry offers better precision and much lower detection limits for fluorescent microspheres than fluorometry because individual fluorescent

colloids are counted, whereas with fluorometry, only the bulk fluorescence of solutions containing fluorescent colloids is measured.

4. It was desirable to use at least two different sizes of CML microspheres in a second set of experiments to determine what size would be the best candidate for use in planned cross-hole field tracer tests in the saturated alluvium at the ATC (site of NC-EWDP-19D1).

5. The alluvium and water from the first set of experiments came from a zone that had a relatively low hydraulic conductivity and a relatively high divalent cation concentration (8-10 mg/L Ca^{2+}), both of which would tend to hinder colloid transport. It was desirable to conduct a second set of experiments using alluvium and water from a high-conductivity zone with a lower divalent cation concentration; i.e., the lowest screened interval in the alluvium in NC-EWDP-19D1 (1-2 mg/L Ca^{2+}). The lower divalent cation concentrations favor colloid stability and transport, so water from this interval would provide a more stringent test of colloid transport in saturated alluvium.

6. Finally, it was desirable to conduct colloid-facilitated Pu transport experiments using the natural colloids collected from NC-EWDP-19D1. Such experiments would provide valuable estimates of colloid-facilitated Pu transport parameters for use in transport process models that feed TSPA. (Pu transport results are not discussed in this analysis report, but are discussed in the model report *Site-Scale Saturated Zone Transport*, (BSC 2003 [162419], Attachment II).

The second set of colloid transport experiments was conducted using alluvium material collected during the drilling of NC-EWDP-19IM1A, at a depth of 785 to 790 ft below land surface. Two 30-cm-long and 2.5-cm-diameter columns were packed with this material. The material was wet-sieved to a size range of 75 to 2000 μm for one of the columns and to a size range of 125 to 2000 μm for the second column. The intent of the slightly different particle-size ranges was to achieve different hydraulic conductivities in the two columns. The column with the smaller particle sizes was expected to have smaller pore throat diameters and, hence, a lower hydraulic conductivity (which is predicted to be heavily influenced by the lower end of the particle-size range) than the other column. The water for the experiments was collected from the lowest screened interval completed in the alluvium in NC-EWDP-19D1, which corresponds to a depth range of approximately 715 to 800 ft below land surface at a distance of 25 to 30 m from NC-EWDP-19IM1A (from which the alluvium material was taken).

The natural colloids were collected from the uppermost screened interval in NC-EWDP-19D1 during the last six weeks of a single-well tracer test conducted in this interval in the spring of 2001. These colloids were analyzed by quantitative x-ray diffraction to be ~95% (by weight) smectite clay, ~4% zeolites, and ~1% other minerals (DTN: LA0306PR831321.001). Definitive determinations of whether this material differed appreciably in composition and origin from the bentonite drilling mud used during the drilling of NC-EWDP-19D1 were inconclusive. The CML microspheres had diameters of 190 nm and 500 nm, and they were tagged with yellow and red fluorescent dyes, respectively. The natural colloids were analyzed by high-sensitivity liquid

in-situ particle spectrometry (HSLIS-S50, Particle Measuring Systems, Inc.), and the fluorescent microspheres were analyzed by flow cytometry (PAS-III, Partec).

The characteristics of the two columns used in the experiments are listed in Table 20. The porosity of both columns was around 40%, and the hydraulic conductivities, somewhat unexpectedly, were initially identical (within measurement error), and both increased significantly during the course of the experiments. The column with the smaller-sized particles had a significantly higher hydraulic conductivity at the end of the experiments. The increase in conductivity/permeability in both columns is attributed to the washing of fine-grained material from the columns and, possibly, to some redistribution of material in the columns over the course of the experiments. The washing of fine-grained material was evident from the continuous background concentrations of colloids in the column effluents during the experiments.

Table 20. Column Parameters in the CML Microsphere and Natural Colloid Experiments

	Length (cm)	Diameter (cm)	Range of Grain Size (microns)	Porosity (%)	Conductivity (cm/s)	Permeability (millidarcy)	Standard Deviation in Permeability (millidarcy)
Column C							
Pre-test (1)	30	2.50	75-2000	38.2	8.81×10^{-3}	9110	432
Post-test (2)	NM	NM	NM	NM	4.21×10^{-2}	43,600	597
Column D							
Pre-test (1)	30	2.50	125-2000	41.0	9.02×10^{-3}	9330	386
Post-test (2)	NM	NM	NM	NM	1.11×10^{-2}	11,500	599

DTN: LA0301AA831352.001.

NOTE: (1) Prior to both experiments in each column.

(2) After both experiments in each column.

The two columns are designated C and D to distinguish them from Columns A and B discussed in Section 6.8.2.1 for the first set of alluvium column experiments.

NM = not measured.

The three different types of colloids were injected along with tritiated water (^{3}HHO) in pulses ranging from 56 to 58 ml in volume. The flow rates in the first set of experiments (one in each column) were ~6 ml/hr, and the flow rates in the second set of experiments were ~1.1 ml/hr. These flow rates resulted in calculated mean residence times of ^{3}HHO in the columns of 8-10 hrs in the first set of experiments and ~50 hrs in the second set. Details of the experimental conditions are provided in Table 21.

Table 21. Experimental Conditions in the CML Microsphere and Natural Colloid Experiments

Experiment	190-nm CML Concentration (mL^{-1})	500-nm CML Concentration (mL^{-1})	Natural Colloid Concentration (mL^{-1})	^{3}HHO Concentration (CPM/mL)	Injection Pulse Volume (mL)	Flow Rate (mL/hr)
Test 1, Column C	3.58×10^{6}	5.82×10^{5}	2.92×10^{10}	1.57×10^{5}	56.70	6.01
Test 1, Column D	3.55×10^{6}	5.78×10^{5}	2.93×10^{10}	1.57×10^{5}	56.02	5.93
Test 2, Column C	3.15×10^{6}	4.97×10^{5}	2.98×10^{10}	4.54×10^{5}	58.25	1.19
Test 2, Column D	3.14×10^{6}	5.13×10^{5}	2.98×10^{10}	4.54×10^{5}	56.94	1.19

DTN: LA0301AA831352.001.

NOTE: CPM = counts per minute.

The experiments were interpreted in the same way as the first set of colloid transport experiments in alluvium-packed columns (i.e., first, the mean residence time and Peclet number of ^{3}HHO in each experiment was determined using the RELAP computer code (STN: 10551-2.0-00), and then colloid filtration rate constants and retardation factors were determined for the colloids assuming that the ^{3}HHO Peclet numbers applied to the colloids). The mean residence times of the colloids were allowed to be adjusted because the colloids broke through the columns significantly earlier than the ^{3}HHO in three of the four experiments. The breakthrough curves of the ^{3}HHO and colloids in each experiment are shown in Figures 17 through 20. Also shown in these figures are the RELAP fits to each data set. The ^{3}HHO and colloid transport parameters obtained from the fits are listed in Table 22.

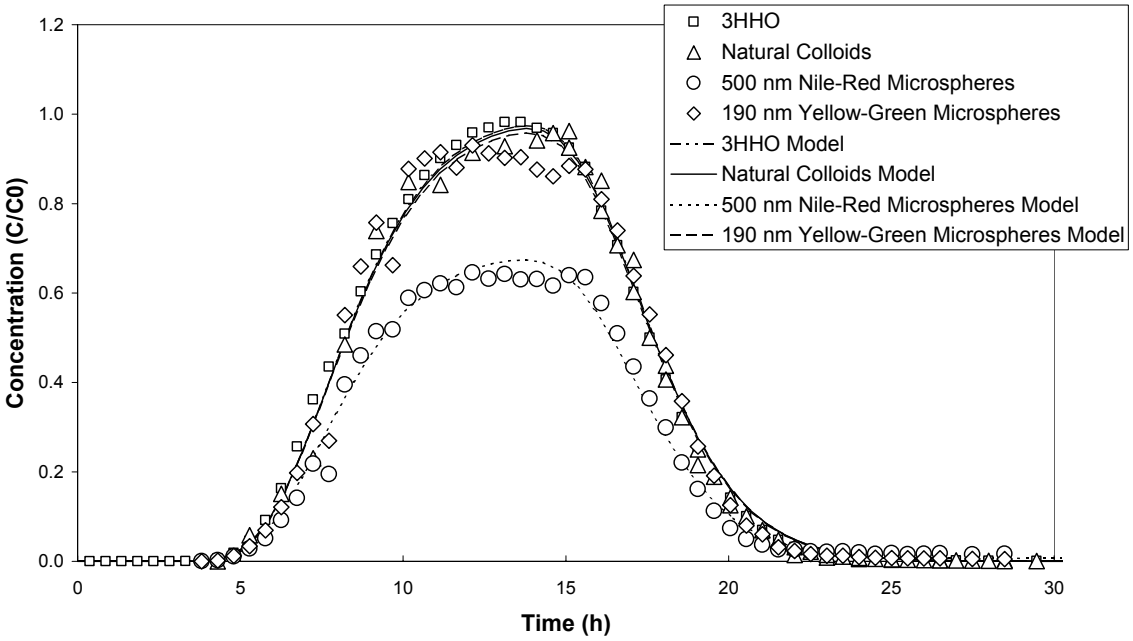

DTN: LA0301AA831352.001; LA0303PR831361.001.

Figure 17. ^{3}HHO and Colloid Breakthrough Curves and RELAP Fits in Test 1, Column C (6.01 mL/hr flow rate)

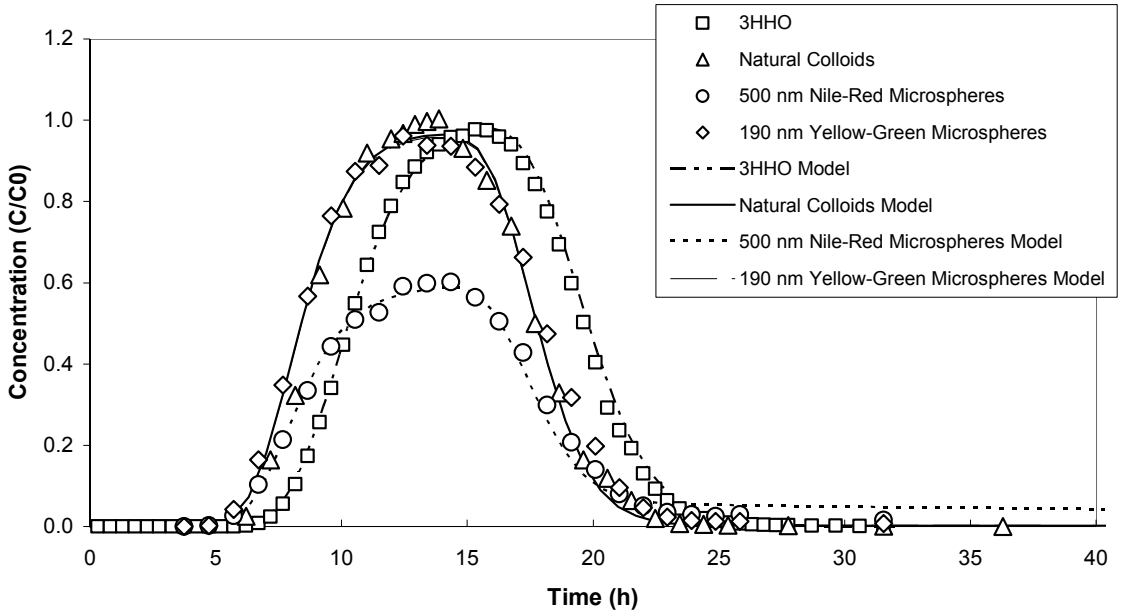

DTN: LA0301AA831352.001; LA0303PR831361.001.

Figure 18. ^{3}HHO and Colloid Breakthrough Curves and RELAP Fits in Test 1, Column D (5.93 mL/hr flow rate)

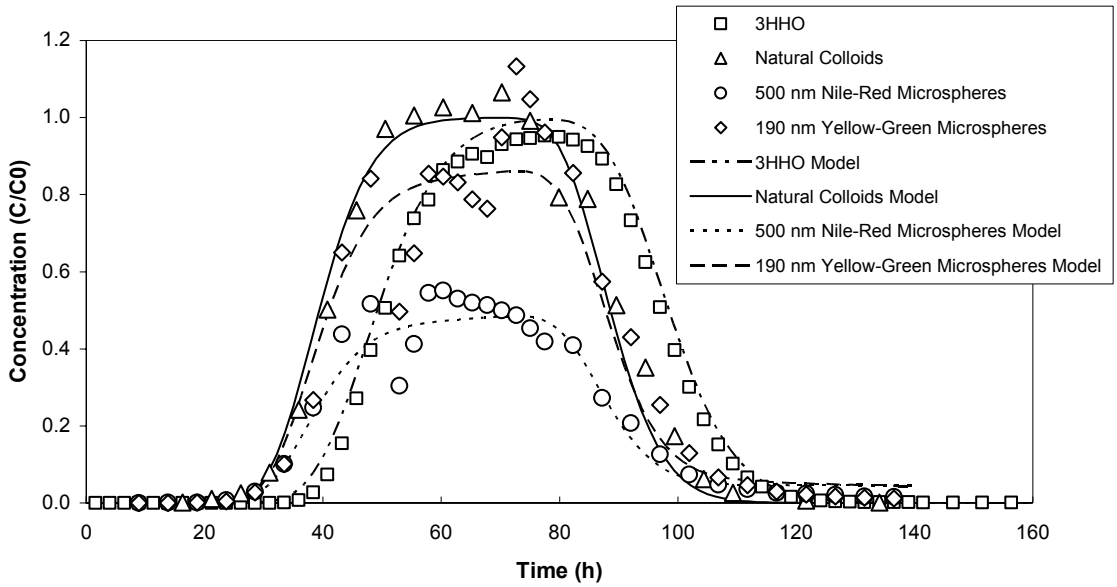

DTN: LA0301AA831352.001 (data); LA0303PR831361.001 (model)

Figure 19. ^{3}HHO and Colloid Breakthrough Curves and RELAP Fits in Test 2, Column C (1.19 mL/hr flow rate)

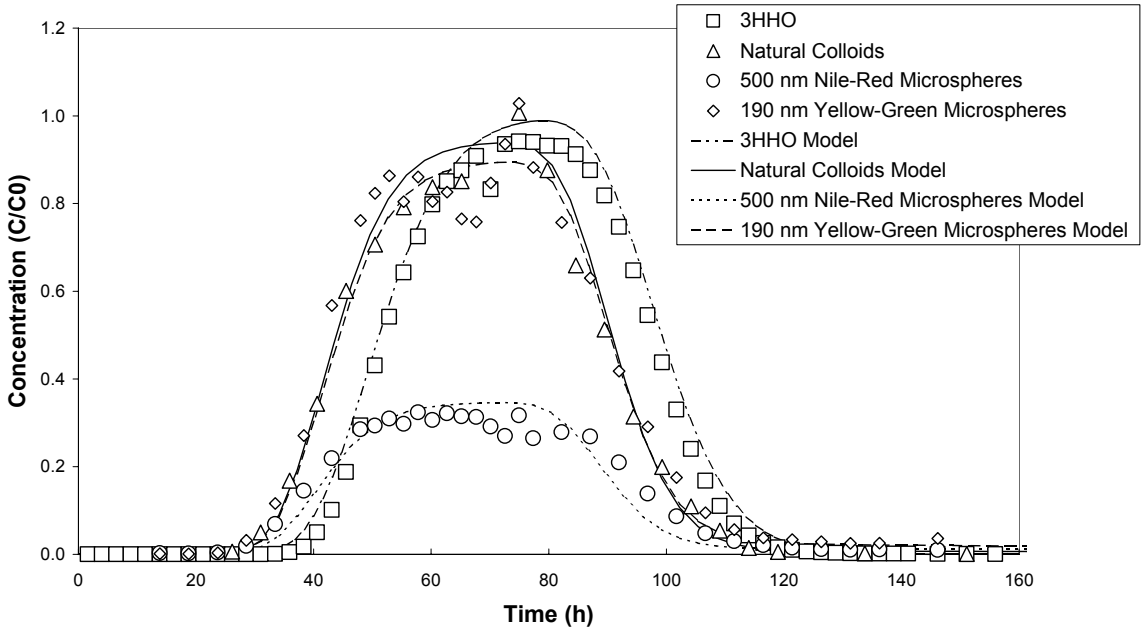

DTN: LA0301AA831352.001 (data); LA0303PR831361.001 (model)

Figure 20. ^{3}HHO and Colloid Breakthrough Curves and RELAP fits in Test 2, Column D (1.19 mL/hr flow rate)

Table 22. Model Parameters from RELAP Fits of Tracer Breakthrough Curves in CML Microsphere and Natural Colloid Experiments in Saturated Alluvium

Model Parameter	Flow Rate (mL/hr), Column			
	6.01, Col. C	5.93, Col. D	1.19, Col. C	1.19, Col. D
^{3}HHO Mean Residence Time (hr)	8.5	10.5	50	52
^{3}HHO (and Colloid) Peclet Number	30	52	64	60
Colloid Mean Residence Time (hr)	8.5	8.5	40	44
190-nm CML Filtration Rate Constant (hr^{-1})	0.002	0.0046	0.0051	0.0029
190-nm CML Retardation Factor	1 (1)	1.5 (1)	1.5	1.5 (1)
500-nm CML Filtration Rate Constant (hr^{-1})	0.045	0.07	0.02	0.025
500-nm CML Retardation Factor	17	4.5	8	35
Natural Colloid Filtration Rate Constant (hr^{-1})	0.0007	0.0039	0	0.0015
Natural Colloid Retardation Factor	1 (1)	1.5 (1)	1 (1)	1.5 (1)

DTN: LA0303PR831361.001.

(1) The RELAP fits for these cases are extremely insensitive to the retardation factor. Any value between 1 and 1000 offers a good fit to the data provided the filtration rate constants are the values listed.

It is apparent from Figures 17 to 20 and Table 22 that both of the CML microspheres transported through the saturated alluvium columns with much less filtration than in the earlier experiments conducted using 330-nm diameter CML and 100-nm diameter silica microspheres (Section 6.8.2.1). The natural colloids also transported with much less filtration than the silica colloids in these experiments. There are two plausible explanations for the significant differences in colloid transport behavior in the two sets of experiments: (1) air bubbles in the columns in the first set of experiments may have significantly attenuated the colloids by providing air-water interfaces that irreversibly trapped the colloids, and (2) the higher divalent cation concentrations in the water used in the earlier experiments may have destabilized the colloids or at least made them more susceptible to attachment to alluvium surfaces. Although the amount of colloid filtration was significantly different in the two sets of alluvium colloid-transport experiments, the results were consistent in that the inorganic colloids transported with similar or less filtration than the CML microspheres in both sets of tests. However, it was also apparent in the second set of experiments that smaller CML microspheres tend to approximate more closely the transport behavior of natural inorganic colloids than larger microspheres in saturated alluvium. This result supports the hypothesis put forth at the end of Section 6.8.2.1 that interception may be a dominant mechanism of colloid filtration in alluvium because of the small pore throat sizes that are present. It also suggests that the smallest detectable CML microspheres should be used in field tracer tests in saturated alluvium to obtain field-scale colloid-transport parameters that are most representative of natural colloids.

6.8.3 Conclusions from CML and Silica Microsphere and Inorganic Colloid Transport Comparisons

Laboratory studies comparing CML and silica-microsphere transport in fractured volcanic rocks indicated that CML microspheres of approximately 300-nm diameter behaved as conservative surrogates for 100-nm diameter silica microspheres in fractured rock. That is, the CML microspheres transported with less attenuation than the silica microspheres in the fractures. Similar tests in columns packed with saturated alluvium indicated that CML microspheres may not necessarily transport with less attenuation than either silica microspheres or natural inorganic colloids in saturated alluvium. Smaller CML microspheres (190-nm diameter) approximated the transport behavior of inorganic colloids better than larger microspheres (330- and 500-nm diameter). The fact that the CML microspheres tended to transport with more attenuation than silica microspheres and natural colloids (primarily smectite clay) in the alluvium column experiments does not negate their usefulness as colloid tracers in field tests. The results of the column experiments involving CML microspheres and natural colloids indicate that microspheres with diameters less than 200 nm should serve as better surrogates for natural colloids than larger microspheres in field tracer tests in alluvium. Even if small CML microspheres transport with somewhat greater attenuation than natural colloids, comparisons of microsphere transport behavior in laboratory and field tracer tests will provide very valuable information on the scale dependence of colloid transport parameters. This information will support further refinement of colloid transport parameter uncertainty distributions in saturated alluvium.

7. CONCLUSIONS

7.1 SUMMARY OF SCIENTIFIC ANALYSIS

This analysis report provides cumulative distribution functions for the uncertainty in the colloid retardation factors in both the saturated volcanics and saturated alluvium for use in TSPA simulations to account for the transport of radionuclides that are irreversibly sorbed to colloids. It also describes a method for calculating a small fraction of colloids (and radionuclides that are irreversibly sorbed to colloids) that transport unretarded through the SZ as a function of groundwater travel time. It is recommended that the combined groundwater travel time through the UZ and SZ (volcanics plus alluvium) be used to obtain an overall fraction of colloids that travels unretarded through the entire natural barrier system.

The transport of colloids is one of the processes that controls the transport of radionuclides through the natural barrier system. Therefore, the process of colloid transport is included in the transport model and is important in evaluating the saturated zone as a barrier for the time scales of interest. The specific acceptance criteria that relate to this report are discussed in Section 4.2.

The use of a retardation factor to describe colloid transport through the SZ implicitly assumes that colloid filtration and detachment rates are fast relative to groundwater travel times through the system. This assumption is shown to be valid for 94+ percent of the colloid mass based on distributions of filtration rate constants from laboratory and field colloid transport experiments.

This analysis report also serves to document laboratory experiments conducted to evaluate the applicability of CML microspheres as field-test surrogates for inorganic colloids in both saturated fractured media and saturated alluvium. In fracture experiments, 330-nm diameter CML microspheres consistently experienced less filtration/attenuation than 100-nm silica colloids. In alluvium-packed column experiments, natural colloids (wide range of diameters, most less than 100 nm) transported with slightly less filtration than 190-nm diameter CML microspheres and with considerably less filtration than 500-nm microspheres. These results suggest that (1) small (<200-nm diameter) CML microspheres may serve as reasonable surrogates for inorganic colloids in saturated alluvium, and (2) CML microspheres may actually serve as conservative colloid tracers in saturated fractured media (yielding transport parameter estimates that result in overprediction of inorganic colloid transport).

7.2 OUTPUTS

Table 23 lists the output data for this scientific analysis report.

Table 23. Output Data

Data Description	Data Tracking Number	Location in Text
Colloid retardation factors for the saturated zone fractured volcanics	LA0303HV831352.002	Table 7
Colloid retardation factors for the saturated zone alluvium	LA0303HV831352.004	Table 8
Fraction of colloids that travel unretarded	LA0303HV831352.003	Table 9

7.3 UNCERTAINTIES

Although results from field colloid transport tests and observations at several contaminated field sites suggest it is reasonable to expect a small fraction of colloid mass to move unretarded through natural systems (Kersting et al. 1999 [103282], p. 56; Penrose et al. 1990 [100811], p. 228), there are uncertainties associated with the assumed partitioning of colloid mass in the SZ into fractions that travel unretarded and retarded. This partitioning is based largely on the assumption that the population of colloids having irreversibly-sorbed radionuclides entering the SZ has a cumulative distribution of filtration rate constants approximately equal to the cumulative distribution of filtration rate constants observed in laboratory and field SZ colloid-transport experiments. Additional uncertainty is introduced as a result of extrapolating the cumulative distribution of observed filtration rate constants to very low probabilities for the purposes of estimating colloid mass fractions that move unretarded. In part to address these large and unquantifiable uncertainties, the distributions of filtration rate constants in the volcanics and alluvium are combined to obtain a single filtration-rate-constant distribution to estimate colloid mass fractions that move unretarded through the entire SZ. The use of a combined distribution for the SZ implicitly assumes a high correlation of filtration rate constants between the volcanics and alluvium, resulting in much higher mass fractions transporting unretarded through the SZ than would be estimated assuming little or no correlation.

Uncertainties are also associated with the retardation factors obtained for both the volcanics and alluvium. Since these retardation factors are used to simulate the transport of irreversibily sorbed radionuclides to colloids, these uncertainties directly relate to the uncertainty of the SZ as a natural barrier. First, all the laboratory and field transport data used to derive the uncertainty distributions were obtained at scales much smaller than the scales of interest for TSPA modeling. Second, the retardation factors derived from many of the transport tests were based on fitting the low colloid concentrations in the tails of breakthrough curves. These tails were sometimes barely above detection or quantification limits, so the fitted retardation factors have considerable uncertainty. However, long tails are virtually always observed whenever analytical methods are sensitive enough to capture them, so they appear to be ubiquitous. Third, there is an implicit assumption that the limited number of combinations of water chemistry, rock mineralogy, and flow conditions tested in the laboratory and field experiments described in this analysis report effectively represents the range of conditions present in the saturated zone as well as the range of conditions that may occur over the 10,000-year performance period. This assumption introduces uncertainty into the distributions obtained for retardation factors. These uncertainties are addressed by (1) assigning lower bounds for retardation factors to cumulative distributions in the volcanics and alluvium such that significant retardation of colloids (seen as long tails in transport tests) always occurs, and (2) assuming that a small fraction of colloid mass moves unretarded through the transport system (as described above) to account for the fact that some finite fraction of colloids always seems to move unretarded in transport tests and is also often observed at contaminated field sites, regardless of scale.

The two sets of laboratory alluvium colloid-transport experiments yielded significantly different results for both CML microsphere and inorganic colloid transport in alluvium. These disparate results, though possibly explainable by the presence of air bubbles in one set of experiments, can be interpreted as imparting a large amount of uncertainty to colloid transport in alluvium. This large uncertainty is preserved by including both sets of experimental results in the overall data

set used to develop the cumulative distributions for colloid-filtration-rate constants and retardation factors in alluvium.

The impact of the uncertainty of the distributions developed in this analysis on Performance Assessment is addressed in the *SZ Flow and Transport Model Abstraction* (BSC 2003 [164870]). Specifically, uncertainty in radionuclide transport is embodied in the breakthrough curves developed in Section 6.6 of the *SZ Flow and Transport Model Abstraction* (BSC 2003 [164870]).

INTENTIONALLY LEFT BLANK

8. INPUTS AND REFERENCES

8.1 DOCUMENTS CITED

The following is a list of the references cited in this document. Column 1 represents the unique six-digit numerical identifier (the Document Input Reference System [DIRS] number), which is placed in the text following the reference callout (e.g., BSC 2002 [155950]). The purpose of these numbers is to assist the reader in locating a specific reference in the DIRS database. Within the reference list, multiple sources by the same author and date (e.g., BSC 2002) are sorted alphabetically by title.

158692 Abdel-Fattah, A.I. and El-Genk, M.S. 1998. "On Colloid Particle Sorption onto a Stagnant Air/Water Interface." *Advances in Colloid and Interface Science*, *78*, 237–266. Amsterdam, The Netherlands: Elsevier. TIC: 253147.

158639 Anghel, I. 2001. *Comparison of Polystyrene and Silica Colloids Transport in Saturated Rock Fractures*. M.S. Thesis. Albuquerque, New Mexico: University of New Mexico. Copyright Requested

144539 Bahr, J.M. and Rubin, J. 1987. "Direct Comparison of Kinetic and Local Equilibrium Formulations for Solute Transport Affected by Surface Reactions." *Water Resources Research, 23,* (3), 438-452. Washington, D.C.: American Geophysical Union. TIC: 246894.

104333 Bales, R.C., Gerba, C.P., Grondin, G.H., and Jensen S.L. 1989. "Bacteriophage Transport in Sandy Soil and Fractured Tuff." *Applied and Environmental Microbiology, 55* (8), 2061–2067. Washington, D.C.: American Society for Microbiology. TIC: 224864.

163935 BSC (Bechtel SAIC Company) 2003. *EBS Radionuclide Transport Abstraction.* ANL-WIS-PA-000001 REV 01A. Las Vegas, Nevada: Bechtel SAIC Company. ACC: MOL.20030617.0222. TBV-5179.

160780 BSC (Bechtel SAIC Company) 2002. *Risk Information to Support Prioritization of Performance Assessment Models.* TDR-WIS-PA-000009 REV 01 ICN 01. Las Vegas, Nevada: Bechtel SAIC Company. ACC: MOL.20021017.0045.

160313 BSC (Bechtel SAIC Company) 2002. *Scientific Processes Guidelines Manual.* MIS-WIS-MD-000001 REV 01. Las Vegas, Nevada: Bechtel SAIC Company. ACC: MOL.20020923.0176.

160146 BSC (Bechtel SAIC Company) 2002. *Total System Performance Assessment-License Application Methods and Approach.* TDR-WIS-PA-000006 REV 00. Las Vegas, Nevada: Bechtel SAIC Company. ACC: MOL.20020923.0175.

158966 BSC (Bechtel SAIC Company) 2002. *The Enhanced Plan for Features, Events, and Processes (FEPs) at Yucca Mountain.* TDR-WIS-PA-000005 REV 00. Las Vegas, Nevada: Bechtel SAIC Company. ACC: MOL.20020417.0385.

162415 BSC (Bechtel SAIC Company) 2003. *Saturated Zone In-Situ Testing.* ANL-NBS-HS-000039 REV 00A. Las Vegas, Nevada: Bechtel SAIC Company. ACC: MOL.20030602.0291.

162649 BSC (Bechtel SAIC Company) 2003. *Site-Scale Saturated Zone Flow Model.* MDL -NBS-HS-000011 REV 01A. Las Vegas, Nevada: Bechtel SAIC Company. ACC: MOL.20030626.0296. TBV-5203

162419 BSC (Bechtel SAIC Company) 2003. *Site-Scale Saturated Zone Transport.* MDL -NBS-HS-000010 REV 01A. Las Vegas, Nevada: Bechtel SAIC Company. ACC: MOL.20030626.0180.

164870 BSC (Bechtel SAIC Company) 2003. *SZ Flow and Transport Model Abstraction.* MDL-NBS-HS-000021 REV 00. Las Vegas, Nevada: Bechtel SAIC Company. ACC: DOC.20030818.0007.

163965 BSC (Bechtel SAIC Company) 2003. *Technical Work Plan For: Saturated Zone Flow and Transport Modeling and Testing.* TWP-NBS-MD-000002 REV 01. Las Vegas, Nevada: Bechtel SAIC Company. ACC: DOC.20030618.0021.

161620 BSC (Bechtel SAIC Company) 2003. *Waste Form and In-Drift Colloids-Associated Radionuclide Concentrations: Abstraction and Summary.* MDL-EBS-PA-000004 REV 00. Las Vegas, Nevada: Bechtel SAIC Company. ACC: DOC.20030626.0006.

161770 Canori, G.F. and Leitner, M.M. 2003. *Project Requirements Document.* TER-MGR-MD-000001 REV 01. Las Vegas, Nevada: Bechtel SAIC Company. ACC: DOC.20030404.0003.

153246 CRWMS M&O (Civilian Radioactive Waste Management System Management and Operations) 2000. *Total System Performance Assessment for the Site Recommendation.* TDR-WIS-PA-000001 REV 00 ICN 01. Las Vegas, Nevada: CRWMS M&O. ACC: MOL.20001220.0045.

153931 CRWMS M&O 2001. *Features, Events, and Processes in SZ Flow and Transport.* ANL-NBS-MD-000002 REV 01. Las Vegas, Nevada: CRWMS M&O. ACC: MOL.20010214.0230.

154365 Freeze, G.A.; Brodsky, N.S.; and Swift, P.N. 2001. *The Development of Information Catalogued in REV00 of the YMP FEP Database*. TDR-WIS-MD-000003 REV 00 ICN 01. Las Vegas, Nevada: Bechtel SAIC Company. ACC: MOL.20010301.0237.

101173 Freeze, R.A. and Cherry, J.A. 1979. *Groundwater.* Englewood Cliffs, New Jersey: Prentice-Hall. TIC: 217571.

109256 Harvey, R.W. and Garabedian, S.P. 1991. "Use of Colloid Filtration Theory in Modeling Movement of Bacteria through a Contaminated Sandy Aquifer." *Environmental Science and Technology, 25*, 178–185. Washington, D.C.: American Chemical Society. TIC: 245733.

117358 Hiemenz, P.C. 1986. *Principles of Colloid and Surface Chemistry*. 2nd Edition, Revised and Expanded. Undergraduate Chemistry Volume 9. Lagowski, J.J., ed. New York, New York: Marcel Dekker. TIC: 246392.

103282 Kersting A. B.; Efurd D. W.; Finnegan D.L.; Rokop D.J.; Smith D.K.; and Thompson, J.L. 1999. "Migration of Plutonium in Groundwater at the Nevada Test Site." *Nature* 397 [6714], 56-59. London, England: Macmillan Journals. TIC: 243597.

162421 Kersting, A.P. and Reimus, P.W., eds. 2003. *Colloid-Facilitated Transport of Low-Solubility Radionuclides: A Field, Experimental, and Modeling Investigation.* UCRL-ID-149688. [Livermore, California]: Lawrence Livermore National Laboratory. TIC: 254176.

163274 NRC (U.S. Nuclear Regulatory Commission) 2003. *Yucca Mountain Review Plan, Final Report.* NUREG-1804, Rev. 2. Washington, D.C.: U.S. Nuclear Regulatory Commission, Office of Nuclear Material Safety and Safeguards. TIC: 254568.

100811 Penrose, W.R.; Polzer, W.L.; Essington, E.H.; Nelson, D.M.; and Orlandini, K.A. 1990. "Mobility of Plutonium and Americium through a Shallow Aquifer in a Semiarid Region." *Environmental Science and Technology, 24*, (2), 228-234. TIC: 224113.

163760 Reimus, P.W. 2003. Laboratory Testing in Support of Saturated Zone Investigations. Scientific Notebook: SN-LANL-SCI-280-V1. ACC: MOL.20030313.0036.

154705 Reimus, P.W. and Haga, M.J. 1999. *Analysis of Tracer Responses in the BULLION Forced-gradient Experiment at Pahute Mesa, Nevada*. LA-13615-MS. Los Alamos, New Mexico: Los Alamos National Laboratory. TIC: 249826.

144579 Valocchi, A.J. 1985. "Validity of the Local Equilibrium Assumption for Modeling Sorbing Solute Transport through Homogeneous Soils." *Water Resources Research, 21,* (6), 808-820. Washington , D.C.: American Geophysical Union. TIC: 223203.

158637 Van de Ven, T.G.M. 1989. "Brownian Motion of Emulsion Droplets." Chapter 2 of *Colloidal Hydrodynamics.* Section 2.1.6. 77-78. New York, New York: Academic Press. TIC: 254717.

163757 Viswanathan, H.V. 2003. Contaminant Transport Modeling of the Saturated Zone at Yucca Mountain, NV. Scientific Notebook: SN-LANL-SCI-297-V1. ACC: MOL.20030609.0493.

114430 Wan, J. and Wilson, J.L. 1994. "Colloid Transport in Unsaturated Porous Media." *Water Resources Research*, *30* (4), 857–864. Washington, D.C.: American Geophysical Union. TIC: 222359.

8.2 CODES, STANDARDS, REGULATIONS, AND PROCEDURES

158535 10 CFR 63. Energy. Disposal of High-Level Radioactive Wastes in a Geologic Repository at Yucca Mountain, Nevada. Readily available.

164105 AP-SI.1Q, Rev. 5, ICN 1. *Software Management.* Washington, D.C.: U.S. Department of Energy, Office of Civilian Radioactive Waste Management. ACC: DOC.20030708.0001.

163021 AP-2.22 Q, Rev 0, ICN 1. *Classification Criteria and Maintenance of the Monitored Geologic Repository Q-List.* Washington, D.C.: Department of Energy, Office of Civilian Radioactive Waste Management. ACC: DOC 20030422.0009.

8.3 SOFTWARE

159065 LANL (Los Alamos National Laboratory) 2002. *RELAP V 2.0*. PC, Windows 2000/NT. 10551-2.0-00

8.4 SOURCE DATA, LISTED BY DATA TRACKING NUMBER

163136 LA0303PR831352.002. Model Interpretations of ER-20-6 Field Tracer Transport Experiment. Submittal date: 03/31/2003.

163137 LA0303PR831352.003. Model Interpretations of NTS Fractured Core Colloid and Colloid-Facilitated Transport Experiments. Submittal date: 03/31/2003.

163138 LA0303PR831352.001. Calculations to Determine Detachment Rate Constant of Microspheres in a Single-Well Tracer Test in Saturated Alluvium. Submittal date: 03/31/2003.

156043 LA0007PR831231.001. Bullfrog Reactive Tracer Test Data. Submittal date: 07/21/2000.

162426 LA0206MH831361.001. Nye County Alluvial Testing Complex Column Experiment ATC Col A NC-EWDP-19D1 25, 8/20/2001. Submittal date: 07/01/2002.

162427 LA0206MH831361.002. Nye County Alluvial Testing Complex Column Experiment ATC Col B NC-EWDP-19D1 25, 8/8/2001. Submittal date: 07/01/2002.

162428 LA0206MH831361.003. Nye County Alluvial Testing Complex Column Experiment ATC Col A NC-EWDP-19D1 25, 11/15/2001. Submittal date: 07/01/2002.

162430 LA0206MH831361.004. Nye County Alluvial Testing Complex Column Experiment ATC Col B NC-EWDP-19D1 25, 11/15/2001. Submittal date: 07/01/2002.

162433 LA0301AA831352.001. Experiments on PU(V)-Colloid Transport in Columns Packed with Material form Nye County Borehole 19D, Zone 4. Submittal date: 01/23/2003.

162434 LA0301PR831352.001. Breakthrough Curves of Iodide, CML Microspheres, and Silica Colloids in Saturated Fractured Cores from the Nevada Test Site. Submittal date: 01/23/2003.

162435 LA0301PR831361.003. Breakthrough Curves of Tritium, Plutonium, and Various Colloids in Saturated UE-20C Fractured Cores from the Nevada Test Site. Submittal date: 01/22/2003.

162436 LA0301PR831361.004. Breakthrough Curves of Tritium, Plutonium, and Various Colloids in Saturated PM-1 and PM-2 Fractured Cores from the Nevada Test Site. Submittal date: 01/22/2003.

162437 LA0302PR831231.002. Solute Data from ER-20-6#2 in the BULLION Forced-Gradient Field Tracer Test at the ER-20-6 Wells at NTS. Submittal date: 02/03/2003.

162438 LA0302PR831231.003. Solute Data from ER-20-6#3 in the BULLION Forced-Gradient Field Tracer Test at the ER-20-6 Wells at NTS. Submittal date: 02/03/2003.

162439 LA0302PR831352.001. Transport of CML Microspheres in Field Tracer Test at ER-20-6#2 Site at the Nevada Test Site (NTS). Submittal date: 03/06/2003.

162440 LA0302PR831352.002. Transport of CML Microspheres in Field Tracer Test at ER-20-6#3 Site at the Nevada Test Site (NTS). Submittal date: 03/06/2003.

163756 LA0303PR831231.003. Model Interpretations of C-Wells Field Tracer Transport Experiments. Submittal date: 03/31/2003

140134 LAPR831231AQ99.001. Prow Pass Reactive Tracer Test Field Data. Submittal date: 02/10/1999.

164492 LA0306PR831321.001. Mineralogy of ATC Colloids and Bentonite Drilling Muds. Submittal date: 06/03/2003.

163135 LA0303PR831361.001. RELAP V2.0 Model Interpretations of Solute and Colloid Transport in Alluvium-Packed Column Transport Experiments. Submittal date: 03/31/2003.

162423 Schijven, J.F.; Hoogenboezem, W.; Hassanizadeh, S.M.; and Peters, J.H. 1999. "Modeling Removal of Bacteriophages MS2 and PRD1 by Dune Recharge at Castricum, Netherlands." *Water Resources Research, 35*, (4), 1101-1111.

8.5 OUTPUT DATA, LISTED BY DATA TRACKING NUMBER

Colloid Retardation Factors for the Saturated Zone Fractured Volcanics. DTN: LA0303HV831352.002

Colloid Retardation Factors for the Saturated Zone Alluvium. DTN: LA0303HV831352.004.

Fraction of Colloids that Travel Unretarded. DTN: LA0303HV831352.003.